A Vertebrate Toxin-Antidote System That Sabotages Mouse Embryogenesis

Duilio M.Z.A. Silva[1*], Morgan Skinner[1], Takaya Totsuka[1], Takashi Akera[1*]

[1]Cell and Developmental Biology Center, National Heart, Lung, and Blood Institute, National Institutes of Health; Bethesda, Maryland 20894, USA

*Corresponding authors. Email: duilio.silva@nih.gov, takashi.akera@nih.gov

Summary

Toxin-antidote (TA) systems are selfish genetic elements that bias their own inheritance by coupling a toxin that kills offspring with an antidote that specifically rescues carriers. Although widespread across bacteria, archaea, fungi, plants, and invertebrates, TA systems have not been described in vertebrates. Here we report the first vertebrate TA system, which sabotages mammalian embryogenesis. We define HEX (Homogenously staining region-mediated Embryo eXecution) as a selfish element that biases its transmission through the female mouse germline. Crosses between HEX heterozygous females and wild-type males result in selective lethality of wild-type embryos, yielding preferential survival of HEX-bearing progeny. Using mouse genetics, embryo transfer, and zygote micromanipulation, we show that HEX operates through a canonical TA mechanism: the maternally deposited toxin SP100 induces genotoxic stress in embryos, while the linked antidote SP110 selectively rescues HEX-positive embryos. Both components are core factors of the interferon signaling pathway, revealing that HEX co-opts innate immune machinery to drive transmission bias. These findings establish a vertebrate TA system and demonstrate that selfish elements can repurpose fundamental cellular pathways to violate Mendelian inheritance, with profound consequences for female fertility.

Introduction

Mendel's Law of Segregation states that each parental allele is randomly transmitted to the next generation. Selfish genetic elements violate this Law by transmitting at a rate above 50%, often at a cost of organismal fitness, including reduced fertility. Although biased transmission of selfish elements has been described across diverse taxa, the underlying molecular mechanisms remain elusive in most systems.[1–6] One strategy used by selfish elements is the toxin-antidote (TA) system, typically composed of a toxin and a genetically linked antidote.[7,8] Selfish DNA encodes a toxin that is distributed to all the gametes in sexually reproducing organisms or to daughter cells in bacteria and archaea. The deposited toxin impairs the development of gametes, embryos, or cells that lack the selfish element, while the ones carrying the selfish DNA survive by expressing an antidote from the TA locus. This mechanism guarantees the increased transmission of the selfish element. TA systems were initially documented four decades ago in bacteria,[9,10] and many have been found in archaea, fungi, invertebrate animals, and plants.[11–20] However, whether such systems operate in vertebrates has remained unknown.

A Homogeneously Staining Region (HSR) on mouse chromosome 1 is a selfish element that exhibits biased transmission, specifically through the female germline.[21,22] The HSR locus contains repetitive DNA composed of segmental duplications of at least two genes, *Sp100-rs* and *Sp110*, that are flanked by single-copy genes, *Sp100* and *Csprs,* on each end (Figure 1A).[23] *Sp100-rs* is a chimeric gene that arose by fusion of the 5' part of *Sp100* and *Csprs*.[23] Speckled Protein (SP) family (e.g., SP100 and SP110) are chromatin readers that perform essential functions in diverse biological processes, including innate immunity,[24–28] but their involvement in genetic conflict has not been explored. Whereas wild-type allele contains ~50 copies of these sequences, the selfish allele expands at least to 800 copies, spanning over 100 Mb (Figure 1A).[29] When HSR heterozygous (H/+) females are crossed with wild-type (+/+) males, approximately half of the +/+ embryos are lost, resulting in a strong transmission bias favoring H/+ offspring. Because HSR is a general cytogenetic term for chromosomal loci with homogeneous staining, we call this selfish element HEX (HSR-mediated Embryo eXecution), evoking a "hex"—a curse—that selectively eliminates wild-type embryos. HEX contrasts with typical selfish elements in the female germline that bias their own segregation to the egg,[30–39] implying that HEX uses a previously unrecognized genetic cheating strategy in mammals.

Results

HEX drives post-implantation lethality of wild-type embryos

Previous study reported biased transmission of HEX, where chromosome 1 with HEX was part of the Robertsonian fusion with chromosome 18,[21] raising the possibility that chromosomal rearrangement contributes to the phenotype. It is essential to disentangle their contribution from that of HEX, since Robertsonian fusions themselves can drive biased transmission in mice and humans.[30,40,41] We therefore directly quantified transmission of the HEX locus in a standard *Mus musculus domesticus* (hereafter, *dom*) genetic background. Crosses

between H/+ females and +/+ males (hereafter, biasing cross or BC in the Figures) yielded 65% H/+ offspring, significantly deviating from the expected Mendelian ratio (Figure 1B and Table 1). This biased transmission was independent of offspring sex (Table 2). These results confirm that selfish HEX autonomously biases its transmission, independent of Robertsonian fusion.

Previous characterization found that +/+ embryos from the biasing cross die between day E4.5 (blastocyst) and E11.5.[21] To precisely define the developmental window of lethality, we performed a high-resolution time course from E1.5 (two-cell) to E11.5 (Figures 1C and 1D). The time course embryo dissection revealed that E7.5 is the time when dead embryos at resorbing sites in the uterus are first observed (Figures 1D–1F). Notably, genotyping by qPCR (quantitative Polymerase Chain Reaction) and FISH (Fluorescence *in situ* Hybridization) showed that genotype ratios become skewed at this stage (Figure 1D, graph), suggesting that selective loss of +/+ embryos at E7.5 underlies HEX transmission bias. Since mouse embryos implant at E4.5–E5.5, selfish HEX kills genetically normal embryos shortly after implantation.

subspecies	dam genotype	sire genotype	H/+ progeny	+/+ progeny	total progeny	% H/+	*P* value
M. m. domesticus	H/+	+/+	187	100	287	65.2	<0.0001*
M. m. musculus	H/+	+/+	108	113	221	48.9	0.7373*

Table 1. HEX transmission bias in *Mus musculus domesticus* and *Mus musculus musculus* backgrounds. *Binomial test (two-tailed) for H/+ to +/+ ratios compared to Mendelian expectations (50:50).

subspecies	dam genotype	sire genotype	H/+ females	+/+ females	total females	H/+ males	+/+ males	total males	*P* value
M. m. domesticus	H/+	+/+	103 (70.1%)	44	147	84 (60%)	56	140	0.0736*

Table 2. HEX transmission bias in females and males of *Mus musculus domesticus*. *Chi-square test (two-tailed) for H/+ to +/+ ratios in females vs males.

Embryo lethality is intrinsic and independent of the uterine environment

Embryos could die either due to internal issues or due to harmful interactions with the maternal environment (i.e., external issues). Because the uterus and the dying embryos have distinct genotypes (H/+ and +/+, respectively), we wished to determine if genetic incompatibility upon implantation was responsible. We performed two distinct embryo transfer experiments. To test if the H/+ uterus can kill healthy ++ embryos, we transferred +/+ embryos that were never exposed to selfish HEX (from the +/+ x +/+ cross) to either H/+ recipient mothers or ++ control (Figure 1G). Transplanted embryos showed indistinguishable survival rates between H/+ and +/+ recipient mothers at E8.5, E11.5, and E17.5 (Figure 1G), implying that the H/+ uterus *per se* is not toxic to +/+ embryos.

To test if biased transmission is independent of uterus genotype, we transferred a mixture of H/+ and +/+ embryos from the biasing cross to +/+ uteri (Figure 1H). Embryo genotyping revealed a biased genotype ratio with 63% H/+ embryos, similar to the natural biasing cross (Figure 1H, graph). Furthermore, 66.5% of the implantation sites had dead embryos, consistent with the idea that embryo death is driving the transmission bias. Together, these results establish that HEX-mediated lethality is embryo-autonomous, indicating that the causal mechanism operates within the embryo rather than through maternal effects.

HEX gene overexpression correlates with transmission bias

To date, the only established mechanism to sabotage/kill genetically wild-type cells/embryos by internal issues is the toxin-antidote (TA) system. The HEX locus encodes several genes (*Sp100*, *Sp110*, *Sp100-rs*, and *Csprs*) (Figure 2A) that could serve as a toxin or an antidote. In addition, the telomere-to-telomere mouse genome assembly[42] found that another SP family gene, *Sp140*, is part of HEX repeats, and our qPCR analysis confirmed that *Sp140* is indeed amplified in mice with HEX (Figure S1). To test if these HEX genes contribute to biased transmission, we first analyzed their expression patterns by RT-qPCR (Reverse Transcription qPCR). RT-qPCR using liver tissues showed that *Sp100*, *Sp110*, and *Sp100-rs* genes were highly expressed in H/+ compared to +/+ (Figure 2B). Interestingly, *Sp100* shows increased expression in H/+ even though it is a single-copy gene in both genotypes. Similarly, we observed overexpression of HEX genes in H/+ oocytes compared to +/+ (Figure 2C). The results raise a possibility that the overexpression of HEX genes mediates biased transmission by embryo killing.

Some meiotic drive systems in *Mus musculus domesticus* become suppressed when introduced to another subspecies, *Mus musculus musculus* (hereafter, *mus*).[35,43] We tested if this applies to our system by backcrossing the HEX locus into the *mus* background for six generations and found that the HEX cheating was completely suppressed (Table 1, *M. m. musculus*). RT-qPCR analyses using *mus* liver and oocytes showed that HEX genes do not overexpress in H/+ compared to +/+ (Figures 2D and 2E), consistent with the idea that HEX gene overexpression contributes to biased transmission.

The HEX locus shows a distinct C-band staining pattern,[44] indicative of heterochromatin.[45] This raised the possibility that heterochromatin regulation modulates HEX gene expression profiles in *dom* vs *mus*. We examined H/+ oocytes from *dom* and *mus* by immunostaining and found that levels of histone H3K9me3, a heterochromatin marker, are significantly higher at the HEX locus in *mus* compared to *dom*, consistent with the HEX gene silencing in the *mus* background (Figure 2F). These results implicate epigenetic silencing as a natural defense against selfish elements.

Toxin candidate is equally distributed to all embryos

142 Embryo transfer experiments and gene expression analyses imply that HEX genes
143 regulate biased transmission, possibly through a TA system. There are at least three main
144 requirements for a TA system to operate in the female germline: (1) the toxin needs to be
145 produced during oogenesis and be deposited to all embryos, (2) the antidote needs to function
146 after fertilization, specifically in the embryos with the selfish element, and (3) when the toxin
147 alone is present in embryos, it must sabotage embryogenesis. It is critical to examine which HEX
148 genes satisfy these requirements to operate a TA system during mammalian reproduction. A key
149 clue emerged from studies of innate immunity in human cells, where SP100 overexpression
150 triggers DNA damage and cell death within the interferon signaling cascade.[28] Notably, co-
151 expression of SP110 suppresses this cytotoxicity.[28] These observations led us to propose that
152 HEX co-opts innate immune factors in the female germline to challenge Mendelian inheritance,
153 with SP100 acting as a toxin and SP110 as its antidote.
154
155 To test the toxin (SP100)–antidote (SP110) hypothesis for HEX cheating, we first
156 examined SP100 protein levels across different tissues. We found that the major isoform of the
157 SP100 protein (68 kDa) is highly expressed in ovaries, compared to liver, spleen, thymus, and
158 testis (Figures 2G and S2). This result is consistent with the first requirement for a TA system,
159 that the toxin is produced during oogenesis. The western blot analysis also showed lower SP100
160 levels in H/+ *mus* ovaries compared to *dom* (Figure 2G, right), consistent with the idea that the
161 *mus* background suppresses the expression of HEX genes to cancel biased transmission. H/+ and
162 +/+ ovaries showed similar SP100 protein levels, but ovaries are composed mostly of non-
163 gamete cells. Therefore, we decided to analyze SP100 levels in more detail at a cellular level,
164 focusing on oocytes and embryos (see below).
165
166 To directly visualize how the toxin candidate, SP100, is deposited in embryos, we
167 analyzed SP100 levels and its localization pattern in oocytes, eggs, and two-cell embryos.
168 Interestingly, meiosis I oocytes from H/+ females did not show higher SP100 levels compared to
169 +/+, but meiosis II eggs and two-cell embryos from H/+ females (biasing cross, BC) showed
170 increased SP100 levels compared to those from +/+ (control cross, CC) (Figures 3A and 3B).
171 Crucially, SP100 levels were equally high in the embryos from the biasing cross regardless of
172 embryo genotype (H/+ and +/+) (Figure S3), consistent with the hypothesis that SP100 toxin is
173 uniformly distributed to all eggs and embryos when cheating happens.
174
175 **Antidote candidate is specifically upregulated in embryos with HEX**
176 A second requirement for TA systems is that the antidote needs to function after
177 fertilization, specifically in the embryos with the selfish element. Indeed, the antidote candidate,
178 SP110, is an established two-cell embryo marker, responding to the zygotic genome activation
179 (ZGA).[25] This expression timing is ideal for SP110 to interact with the maternally deposited
180 toxin candidate, SP100, to suppress its toxicity. To test if embryos with selfish HEX show higher
181 SP110 levels compared to the dying +/+ embryos, we analyzed late two-cell embryos that have
182 likely completed ZGA. Our analysis showed that H/+ embryos have significantly higher nuclear

183 SP110 levels compared to +/+ embryos in the biasing cross (Figure 3C), consistent with the
184 hypothesis. The SP110 level in +/+ embryos from the biasing cross was similar to that of +/+
185 embryos from the control cross (Figure 3C), suggesting that while +/+ embryos show basal
186 SP110 expression, H/+ embryos overexpress SP110, likely due to their higher gene-copy
187 number, and thus specifically neutralize the toxic effect. These results show that SP110 meets the
188 requirement to serve as an antidote in the HEX system.
189
190 Our model predicts that HEX-mediated toxicity is suppressed upon paternal transmission.
191 While the SP100 toxin is maternally deposited into all embryos, the antidote SP110 is expressed
192 after fertilization. Thus, embryos inheriting HEX—even from sperm—can express SP110 and
193 neutralize the toxin. Consistent with the model, previous study have shown that transmission bias
194 is canceled when crossing H/+ females with H/H males.[21] Furthermore, the asymmetric
195 contribution of toxin explains why transmission bias is restricted to the female germline.
196
197 **Dying +/+ embryos have increased DNA damage**
198 A third requirement for a TA system is that a toxic effect occur in embryos when the
199 toxin is not suppressed by an antidote. Since SP100 overexpression causes increased DNA
200 damage in human cells,[28] we asked if dying +/+ embryos exhibit elevated DNA damage. We
201 examined a DNA damage marker, 53BP1,[46] in embryonic cells from day E6.5, one day prior to
202 the onset of +/+ embryo death. The immunofluorescence analysis showed that +/+ embryos from
203 the biasing cross have higher levels of DNA damage compared to H/+ embryos from the same
204 cross and +/+ embryos from the control cross (Figure 4A), linking SP100 activity with
205 genotoxicity and embryo killing.
206
207 **SP100 and SP110 compose a minimal TA module**
208 To directly test if SP100 and SP110 are sufficient to operate a TA system during mouse
209 embryogenesis, we ectopically expressed them by microinjecting their cRNA into +/+ zygotes
210 from the control cross and cultured the embryos for three days (E3.5, the morula stage) (Figure
211 4B). SP100 alone potently disrupted embryogenesis in a dose-dependent manner, inducing
212 developmental arrest and DNA damage. Co-expression of SP110 suppressed these defects
213 without altering SP100 levels, demonstrating functional neutralization (Figures 4B–4C). We
214 noticed that SP100-expressing embryos often show DNA bridges, which may be the origin of the
215 DNA damage (Figure S4), consistent with the observation in human cells.[28] These results
216 establish SP100 and SP110 as a minimal toxin–antidote pair capable of recapitulating HEX
217 activity.
218
219 We also tested whether other genes on the HEX locus, *Sp100-rs* and *Sp140*, impact
220 embryogenesis when overexpressed. While SP100-rs overexpression did not impact
221 embryogenesis (Figure S5A), SP140 overexpression had mild toxic effects (Figure 4B), possibly
222 contributing as a secondary toxin. However, SP140 levels are similar between the control and
223 biasing crosses in two-cell embryos (Figure S6A), suggesting that SP140 is not a primary toxin

224 and that SP100–SP110 constitutes the core functional module.
225
226 **Discussion**
227 **A vertebrate toxin-antidote system that repurposes innate immune mechanisms**
228 Our findings represent the first canonical toxin-antidote system in vertebrates and the first
229 genetic cheating mechanism that exploits the DNA damage pathway. Together with a previous
230 report investigating a TA system in *C. elegans* that delays larval development,[20] subverting
231 embryogenesis may be a common strategy for TA systems in animals. Notably, both toxin and
232 antidote for the HEX system derive from the interferon signaling pathway, suggesting that innate
233 immune components can be repurposed to enforce selfish transmission. This study expands the
234 conceptual framework of genetic conflict by showing that core cellular defense pathways can be
235 redirected toward intragenomic competition.
236
237 **Temporal gating of toxicity**
238 Our HEX TA model (Figure 5) proposes that H/+ females poison their embryos by
239 increasing SP100 protein levels in meiosis II eggs. Some mRNAs that are critical for oocyte
240 maturation and early development exhibit dormancy in oocytes and only initiate translation in
241 eggs and embryos.[47] *Sp100* mRNA may be employing a similar mechanism to produce toxin at
242 the right place at the right time. It is also important to consider why the SP100 toxin, which is
243 already upregulated in the two-cell stage, kills wild-type embryos only at day E6.5–7.5. We
244 speculate on two possibilities. First, SP100 may lack critical cofactors to induce DNA damage
245 during early embryogenesis. Indeed, human SP100 requires a nuclear body, the PML body, to
246 induce DNA damage,[28] and the PML body is absent from oocytes and early embryos and only
247 starts forming at the morula stage.[48] This delayed formation of the PML body can explain why
248 SP100 does not immediately kill embryos after fertilization. Second, SP100 may cause mild
249 DNA damage in early embryos, which only triggers death after implantation. Consistent with
250 this model, previous work has shown that embryos become particularly sensitive to mild DNA
251 damage, resulting in apoptosis at E6.5 when gastrulation takes place.[49] Furthermore, multiple
252 mutant mouse lines with elevated DNA damage during embryogenesis show lethality at E6.5–
253 E7.5,[49–53] consistent with our model that HEX kills embryos via DNA damage.
254
255 **Evolutionary dynamics of suppression and innovation**
256 HEX activity is fully suppressed in the *M. m. musculus* background likely through
257 heterochromatin-mediated silencing, illustrating a host defense mechanism against selfish
258 elements (Table 1 and Figure 2).[54] Some *M. m. musculus* populations carry a structural variant of
259 HEX element called "double-band", composed of two conspicuous heterochromatic bands
260 originating from a paracentric inversion involving the HEX locus. Remarkably, the double-band
261 cheats during meiosis by biased segregation to the egg.[43,55] These observations raise an intriguing
262 possibility that HEX escaped the suppression in *M. m. musculus* by evolving a new cheating
263 strategy in a distinct arena: asymmetric female meiosis. This highlights the evolutionary
264 plasticity of genetic conflict systems.
265

TA systems cause intragenomic conflict between the selfish element and the rest of the genome, facilitating genome innovation. Thus, investigating the HEX TA system would also provide a unique window to dissect how such conflicts have shaped mammalian genome, development, and reproduction.

Limitations of the Study

Although our RT-qPCR analyses distinguish *Sp100* and *Sp100-rs* transcripts, the SP100 antibody used in this study may also recognize SP100-rs, if it is expressed as a protein. Thus, the immunofluorescence signals in Figures 3A and 3B could, in principle, include contributions from SP100-rs. However, SP100-rs lacks the C-terminal region of SP100, including the nuclear localization signal (NLS) (Figure S6B), and correspondingly displays diffuse localization in embryos when expressed as a GFP fusion (Figure S5B). Therefore, we consider that the increased nuclear enrichment of SP100 in embryos from H/+ females is indeed the full-length SP100 with intact NLS rather than SP100-rs (Figure 3B).

References

1. Lindholm, A.K., Dyer, K.A., Firman, R.C., Fishman, L., Forstmeier, W., Holman, L., Johannesson, H., Knief, U., Kokko, H., Larracuente, A.M., et al. (2016). The Ecology and Evolutionary Dynamics of Meiotic Drive. Trends in Ecology & Evolution *31*, 315–326. https://doi.org/10.1016/j.tree.2016.02.001.

2. Kruger, A.N., and Mueller, J.L. (2021). Mechanisms of meiotic drive in symmetric and asymmetric meiosis. Cellular and molecular life sciences : CMLS *78*, 3205–3218. https://doi.org/10.1007/s00018-020-03735-0.

3. Clark, F.E., and Akera, T. (2021). Unravelling the mystery of female meiotic drive: where we are. Open biology *11*, 210074. https://doi.org/10.1098/rsob.210074.

4. Arora, U.P., and Dumont, B.L. (2022). Meiotic drive in house mice: mechanisms, consequences, and insights for human biology. Chromosome research *30*, 165–186. https://doi.org/10.1007/s10577-022-09697-2.

5. Chmátal, L., Schultz, R.M., Black, B.E., and Lampson, M.A. (2017). Cell Biology of Cheating—Transmission of Centromeres and Other Selfish Elements Through Asymmetric Meiosis. In Centromeres and Kinetochores (Springer, Cham), pp. 377–396. https://doi.org/10.1007/978-3-319-58592-5_16.

6. Helleu, Q., Gérard, P.R., and Montchamp-Moreau, C. (2014). Sex chromosome drive. Cold Spring Harbor perspectives in biology *7*, a017616. https://doi.org/10.1101/cshperspect.a017616.

7. Burga, A., Ben-David, E., and Kruglyak, L. (2020). Toxin-Antidote Elements Across the Tree of Life. Annu Rev Genet *54*, 387–415. https://doi.org/10.1146/annurev-genet-112618-043659.

8. LeRoux, M., and Laub, M.T. (2022). Toxin-Antitoxin Systems as Phage Defense Elements. Annu. Rev. Microbiol. *76*, 21–43. https://doi.org/10.1146/annurev-micro-020722-013730.

9. Ogura, T., and Hiraga, S. (1983). Mini-F plasmid genes that couple host cell division to plasmid proliferation. Proc Natl Acad Sci U S A *80*, 4784–4788. https://doi.org/10.1073/pnas.80.15.4784.

10. Gerdes, K., Rasmussen, P.B., and Molin, S. (1986). Unique type of plasmid maintenance function: postsegregational killing of plasmid-free cells. Proc Natl Acad Sci U S A *83*, 3116–3120. https://doi.org/10.1073/pnas.83.10.3116.

11. Beeman, R.W., Friesen, K.S., and Denell, R.E. (1992). Maternal-effect selfish genes in flour beetles. Science *256*, 89–92. https://doi.org/10.1126/science.1566060.

12. Beeman, R.W., and Friesen, K.S. (1999). Properties and natural occurrence of maternal-effect selfish genes (“Medea” factors) in the red flour beetle, tribolium castaneum. Heredity (Edinb) *82 (Pt 5)*, 529–534. https://doi.org/10.1038/sj.hdy.6885150.

13. Seidel, H.S., Ailion, M., Li, J., van Oudenaarden, A., Rockman, M.V., and Kruglyak, L. (2011). A novel sperm-delivered toxin causes late-stage embryo lethality and transmission ratio distortion in C. elegans. PLoS Biol *9*, e1001115. https://doi.org/10.1371/journal.pbio.1001115.

14. Turner, B.C., and Perkins, D.D. (1979). Spore Killer, a Chromosomal Factor in Neurospora That Kills Meiotic Products Not Containing It. Genetics *93*, 587–606.

15. Rhoades, N.A., Harvey, A.M., Samarajeewa, D.A., Svedberg, J., Yusifov, A., Abusharekh, A., Manitchotpisit, P., Brown, D.W., Rehard, D.G., Peters, J., et al. (2019). Identification of rfk-1, a meiotic driver undergoing RNA editing in Neurospora. Genetics *212*, 309–438. https://doi.org/10.1534/genetics.119.302122.

16. Nuckolls, N.L., Nidamangala Srinivasa, A., Mok, A.C., Helston, R.M., Bravo Núñez, M.A., Lange, J.J., Gallagher, T.J., Seidel, C.W., and Zanders, S.E. (2022). S. pombe wtf drivers use dual transcriptional regulation and selective protein exclusion from spores to cause meiotic drive. PLoS Genet *18*, e1009847. https://doi.org/10.1371/journal.pgen.1009847.

17. Takagi, H., Kakuta, Y., Okada, T., Yao, M., Tanaka, I., and Kimura, M. (2005). Crystal structure of archaeal toxin-antitoxin RelE-RelB complex with implications for toxin activity and antitoxin effects. Nat Struct Mol Biol *12*, 327–331. https://doi.org/10.1038/nsmb911.

18. Yang, J., Zhao, X., Cheng, K., Du, H., Ouyang, Y., Chen, J., Qiu, S., Huang, J., Jiang, Y., Jiang, L., et al. (2012). A killer-protector system regulates both hybrid sterility and segregation distortion in rice. Science *337*, 1336–1340. https://doi.org/10.1126/science.1223702.

19. Ben-David, E., Burga, A., and Kruglyak, L. (2017). A maternal-effect selfish genetic element in Caenorhabditis elegans. Science *356*, 1051–1055. https://doi.org/10.1126/science.aan0621.

20. Pliota, P., Marvanova, H., Koreshova, A., Kaufman, Y., Tikanova, P., Krogull, D., Hagmüller, A., Widen, S.A., Handler, D., Gokcezade, J., et al. (2024). Selfish conflict underlies RNA-mediated parent-of-origin effects. Nature *628*, 122–129. https://doi.org/10.1038/s41586-024-07155-z.

21. Weichenhan, D., Traut, W., Kunze, B., and Winking, H. (1996). Distortion of Mendelian recovery ratio for a mouse HSR is caused by maternal and zygotic effects. Genetical Research *68*, 125–129. https://doi.org/10.1017/S0016672300034017.

22. Traut, W., Winking, H., and Adolph, S. (1984). An extra segment in chromosome 1 of wild Mus musculus: a C-band positive homogeneously staining region. Cytogenetics and cell genetics *38*, 290–297. https://doi.org/10.1159/000132077.

23. Traut, W., Rahn, I.M., Winking, H., Kunze, B., and Weichenhan, D. (2001). Evolution of a 6-200 Mb long-range repeat cluster in the genus Mus. Chromosoma *110*, 247–252. https://doi.org/10.1007/s004120100152.

24. Fraschilla, I., and Jeffrey, K.L. (2020). The Speckled Protein (SP) Family: Immunity's Chromatin Readers. Trends in immunology *41*, 572–585. https://doi.org/10.1016/j.it.2020.04.007.

25. Guo, Y., Kitano, T., Inoue, K., Murano, K., Hirose, M., Li, T.D., Sakashita, A., Ishizu, H., Ogonuki, N., Matoba, S., et al. (2024). Obox4 promotes zygotic genome activation upon loss of Dux. Elife *13*, e95856. https://doi.org/10.7554/eLife.95856.

26. Witt, K.C., Dziulko, A., An, J., Pekovic, F., Cheng, A.X., Liu, G.Y., Lee, O.V., Turner, D.J., Lari, A., Gaidt, M.M., et al. (2025). SP140–RESIST pathway regulates interferon mRNA stability and antiviral immunity. Nature *643*, 1372–1380. https://doi.org/10.1038/s41586-025-09152-2.

27. Ji, D.X., Witt, K.C., Kotov, D.I., Margolis, S.R., Louie, A., Chevée, V., Chen, K.J., Gaidt, M.M., Dhaliwal, H.S., Lee, A.Y., et al. (2021). Role of the transcriptional regulator SP140 in resistance to bacterial infections via repression of type I interferons. eLife *10*, 1–22. https://doi.org/10.7554/eLife.67290.

28. Aird, E.J., Rabl, J., Knuesel, T., Groen, K., Awwad, S.W., Korablev, B., Scherpe, L., Al-Herz, W., Hupfer, R., Recher, M., et al. (2026). An SP110–SP100 axis is a critical regulator of promyelocytic leukaemia body dynamics and mitotic fidelity. Nat Cell Biol, 1–12. https://doi.org/10.1038/s41556-026-01916-w.

29. Agulnik, S., Plass, C., Traut, W., and Winking, H. (1993). Evolution of a long-range repeat family in Chromosome 1 of the genus Mus. Mammalian Genome *4*, 704–710. https://doi.org/10.1007/BF00357793.

30. Chmátal, L., Gabriel, S.I., Mitsainas, G.P., Martínez-Vargas, J., Ventura, J., Searle, J.B., Schultz, R.M., and Lampson, M.A. (2014). Centromere strength provides the cell biological basis for meiotic drive and karyotype evolution in mice. Current Biology *24*, 2295–2300. https://doi.org/10.1016/j.cub.2014.08.017.

31. Iwata-Otsubo, A., Dawicki-McKenna, J.M., Akera, T., Falk, S.J., Chmátal, L., Yang, K., Sullivan, B.A., Schultz, R.M., Lampson, M.A., and Black, B.E. (2017). Expanded Satellite Repeats Amplify a Discrete CENP-A Nucleosome Assembly Site on Chromosomes that Drive in Female Meiosis. Current Biology *27*, 2365-2373.e8. https://doi.org/10.1016/j.cub.2017.06.069.

32. Akera, T., Chmátal, L., Trimm, E., Yang, K., Aonbangkhen, C., Chenoweth, D.M., Janke, C., Schultz, R.M., and Lampson, M.A. (2017). Spindle asymmetry drives non-Mendelian chromosome segregation. Science (New York, N.Y.) *358*, 668–672. https://doi.org/10.1126/science.aan0092.

33. Wu, T., Lane, S.I.R., Morgan, S.L., and Jones, K.T. (2018). Spindle tubulin and MTOC asymmetries may explain meiotic drive in oocytes. Nature Communications *9*, 2952. https://doi.org/10.1038/s41467-018-05338-7.

34. Dawe, R.K., Lowry, E.G., Gent, J.I., Stitzer, M.C., Swentowsky, K.W., Higgins, D.M., Ross-Ibarra, J., Wallace, J.G., Kanizay, L.B., Alabady, M., et al. (2018). A Kinesin-14 Motor Activates Neocentromeres to Promote Meiotic Drive in Maize. Cell *173*, 839-850.e18. https://doi.org/10.1016/j.cell.2018.03.009.

35. Didion, J.P., Morgan, A.P., Clayshulte, A.M.-F., Mcmullan, R.C., Yadgary, L., Petkov, P.M., Bell, T.A., Gatti, D.M., Crowley, J.J., Hua, K., et al. (2015). A multi-megabase copy number gain causes maternal transmission ratio distortion on mouse chromosome 2. PLoS genetics *11*, e1004850. https://doi.org/10.1371/journal.pgen.1004850.

36. Fishman, L., and Saunders, A. (2008). Centromere-associated female meiotic drive entails male fitness costs in monkeyflowers. Science (New York, N.Y.) *322*, 1559–1562. https://doi.org/10.1126/science.1161406.

37. Hanlon, S.L., and Hawley, R.S. (2023). B chromosomes reveal a female meiotic drive suppression system in *Drosophila melanogaster*. Current Biology *33*, 2300-2306.e5. https://doi.org/10.1016/j.cub.2023.04.028.

38. Clark, F.E., Conte, M.A., and Kocher, T.D. (2018). Genomic Characterization of a B Chromosome in Lake Malawi Cichlid Fishes. Genes *9*. https://doi.org/10.3390/genes9120610.

39. Hewitt, G.M. (1976). Meiotic drive for B-chromosomes in the primary oocytes of Myrmeleotettix maculatus (Orthopera: Acrididae). Chromosoma *56*, 381–391. https://doi.org/10.1007/BF00292957.

40. Gropp, A., Winking, H., Redi, C., Capanna, E., Britton-Davidian, J., and Noack, G. (1982). Robertsonian karyotype variation in wild house mice from Rhaeto-Lombardia. Cytogenet Cell Genet *34*, 67–77. https://doi.org/10.1159/000131794.

41. Pardo-Manuel de Villena, F., and Sapienza, C. (2001). Female Meiosis Drives Karyotypic Evolution in Mammals. Genetics *159*, 1179–1189.

42. Francis, B.A., Gozashti, L., Costello, K., Kasahara, T., Harringmeyer, O.S., Lilue, J., Wu, T., Zoltowska, K., Helmy, M., Kato, T., et al. (2025). Complete genome assemblies of two mouse subspecies reveal structural diversity of telomeres and centromeres. Nat Genet *57*, 2852–2862. https://doi.org/10.1038/s41588-025-02367-z.

43. Agulnik, S.I., Sabantsev, I.D., Orlova, G.V., and Ruvinsky, A.O. (1993). Meiotic drive on aberrant chromosome 1 in the mouse is determined by a linked distorter. Genetical research *61*, 91–96. https://doi.org/10.1017/s0016672300031189.

44. Winking, H., Weith, A., Boldyreff, B., Moriwaki, K., Fredga, K., and Traut, W. (1991). Polymorphic HSRs in chromosome 1 of the two semispecies Mus musculus musculus and M. m. domesticus have a common origin in an ancestral population. Chromosoma *100*, 147–151. https://doi.org/10.1007/BF00337242.

45. Sumner, A.T. (1972). A simple technique for demonstrating centromeric heterochromatin. Exp Cell Res *75*, 304–306. https://doi.org/10.1016/0014-4827(72)90558-7.

46. Paiano, J., Zolnerowich, N., Wu, W., Pavani, R., Wang, C., Li, H., Zheng, L., Shen, B., Sleckman, B.P., Chen, B.-R., et al. (2021). Role of 53BP1 in end protection and DNA synthesis at DNA breaks. Genes Dev *35*, 1356–1367. https://doi.org/10.1101/gad.348667.121.

47. Lorenzo-Orts, L., and Pauli, A. (2024). The molecular mechanisms underpinning maternal mRNA dormancy. Biochem Soc Trans *52*, 861–871. https://doi.org/10.1042/BST20231122.

48. Udagawa, O., Kato-Udagawa, A., and Hirano, S. (2022). Promyelocytic leukemia nuclear body-like structures can assemble in mouse oocytes. Biology open *11*. https://doi.org/10.1242/bio.059130.

49. Heyer, B.S., MacAuley, A., Behrendtsen, O., and Werb, Z. (2000). Hypersensitivity to DNA damage leads to increased apoptosis during early mouse development. Genes Dev *14*, 2072–2084.

50. Tebbs, R.S., Flannery, M.L., Meneses, J.J., Hartmann, A., Tucker, J.D., Thompson, L.H., Cleaver, J.E., and Pedersen, R.A. (1999). Requirement for the Xrcc1 DNA base excision repair gene during early mouse development. Dev Biol *208*, 513–529. https://doi.org/10.1006/dbio.1999.9232.

51. Gurley, K.E., and Kemp, C.J. (2001). Synthetic lethality between mutation in Atm and DNA-PK(cs) during murine embryogenesis. Curr Biol *11*, 191–194. https://doi.org/10.1016/s0960-9822(01)00048-3.

52. Henrie, M.S., Kurimasa, A., Burma, S., Ménissier-de Murcia, J., de Murcia, G., Li, G.C., and Chen, D.J. (2003). Lethality in PARP-1/Ku80 double mutant mice reveals physiological synergy during early embryogenesis. DNA Repair (Amst) *2*, 151–158. https://doi.org/10.1016/s1568-7864(02)00199-4.

452 53. Juan, H.-C., Lin, Y., Chen, H.-R., and Fann, M.-J. (2016). Cdk12 is essential for embryonic
453 development and the maintenance of genomic stability. Cell Death Differ *23*, 1038–1048.
454 https://doi.org/10.1038/cdd.2015.157.

455 54. Torgunakov, N.Y., Kizilova, E.A., Karamysheva, T.V., Malinovskaya, L.P., Bikchurina, T.I.,
456 and Borodin, P.M. (2021). Homogeneously Staining Regions (HSR) in Chromosome 1 of the
457 House Mouse: Synapsis and Recombination at Meiosis. Cytogenetic and Genome Research
458 *161*, 14–22. https://doi.org/10.1159/000513266.

459 55. Agulnik, S.I., Agulnik, A.I., and Ruvinsky, A.O. (1990). Meiotic drive in female mice
460 heterozygous for the HSR inserts on chromosome 1. Genetical research *55*, 97–100.
461 https://doi.org/10.1017/s0016672300025325.

462 56. Weichenhan, D., Kunze, B., Winking, H., van Geel, M., Osoegawa, K., de Jong, P.J., and
463 Traut, W. (2001). Source and component genes of a 6-200 Mb gene cluster in the house
464 mouse. Mamm Genome *12*, 590–594. https://doi.org/10.1007/s00335-001-3015-9.

465 57. Behringer, R., Gertsenstein, M., Nagy, K.V., and Nagy, A. (2013). Assisted reproduction. In
466 Manipulating the Mouse Embryo: A Laboratory Manual (Cold Spring Harbor Laboratory
467 Press), pp. 608–613.

468 58. Shea, K., and Geijsen, N. (2007). Dissection of 6.5 dpc mouse embryos. J Vis Exp, 160.
469 https://doi.org/10.3791/160.

470 59. Truett, G.E., Heeger, P., Mynatt, R.L., Truett, A.A., Walker, J.A., and Warman, M.L. (2000).
471 Preparation of PCR-quality mouse genomic DNA with hot sodium hydroxide and tris
472 (HotSHOT). Biotechniques *29*, 52, 54. https://doi.org/10.2144/00291bm09.

473 60. Bel, Y., Ferré, J., and Escriche, B. (2011). Quantitative real-time PCR with SYBR Green
474 detection to assess gene duplication in insects: study of gene dosage in Drosophila
475 melanogaster (Diptera) and in Ostrinia nubilalis (Lepidoptera). BMC Res Notes *4*, 84.
476 https://doi.org/10.1186/1756-0500-4-84.

477 61. Kõressaar, T., Lepamets, M., Kaplinski, L., Raime, K., Andreson, R., and Remm, M. (2018).
478 Primer3_masker: integrating masking of template sequence with primer design software.
479 Bioinformatics *34*, 1937–1938. https://doi.org/10.1093/bioinformatics/bty036.

480 62. Dozortsev, D.I., and McGinnis, K.T. (2001). An improved fixation technique for
481 fluorescence in situ hybridization for preimplantation genetic diagnosis. Fertil Steril *76*, 186–
482 188. https://doi.org/10.1016/s0015-0282(01)01836-2.

483 63. Yu, G., Ma, S., Zhu, Y., Liu, Y., Zhang, H., Wu, K., and Hao, A. (2020). Application of
484 improved single blastomere fixation technique in preimplantation genetic diagnosis.
485 Cytotechnology *72*, 217–226. https://doi.org/10.1007/s10616-020-00371-1.

486 64. Clark, F.E., Silva, D.M.Z.A., Skinner, M., Rosin, L.F., Greenberg, N.L., and Akera, T.
487 (2025). Whole Mount Oligopaint Fluorescence In Situ Hybridization of Mouse Oocytes,
488 Eggs, or Early-Stage Embryos. Methods Mol Biol *2946*, 69–86. https://doi.org/10.1007/978-
489 1-0716-4658-8_6.

65. Igarashi, H., Knott, J.G., Schultz, R.M., and Williams, C.J. (2007). Alterations of PLCbeta1 in mouse eggs change calcium oscillatory behavior following fertilization. Developmental biology *312*, 321–330. https://doi.org/10.1016/j.ydbio.2007.09.028.

66. Ye, J., Coulouris, G., Zaretskaya, I., Cutcutache, I., Rozen, S., and Madden, T.L. (2012). Primer-BLAST: a tool to design target-specific primers for polymerase chain reaction. BMC Bioinformatics *13*, 134. https://doi.org/10.1186/1471-2105-13-134.

67. Kubista, M., and Sindelka, R. (2007). The Prime Technique. GIT Lab J Eur.

68. Livak, K.J., and Schmittgen, T.D. (2001). Analysis of Relative Gene Expression Data Using Real-Time Quantitative PCR and the 2−ΔΔCT Method. Methods *25*, 402–408. https://doi.org/10.1006/meth.2001.1262.

69. Xie, F., Wang, J., and Zhang, B. (2023). RefFinder: a web-based tool for comprehensively analyzing and identifying reference genes. Funct Integr Genomics *23*, 125. https://doi.org/10.1007/s10142-023-01055-7.

70. Callicott, R.J., and Womack, J.E. (2006). Real-time PCR assay for measurement of mouse telomeres. Comp Med *56*, 17–22.

Resource availability:

Lead contact

Further information and requests for resources and reagents should be directed to and will be fulfilled by the lead contact, Takashi Akera (takashi.akera@nih.gov).

Materials availability

The microscopy and western blot data required to reproduce the results in the study will be publicly available in Figshare upon publication. Any additional information required to reanalyze the data reported in this paper is available from the corresponding authors upon request.

Data and code availability

- All original codes are available in this study's Supplementary Text.
- Any additional information required to reanalyze the data reported in this paper is available from the lead contact upon request.

Acknowledgments: We thank M. Lichten and J.L. Mueller for comments on the manuscript, Akera lab members for discussion, N. Altan-Bonnet, Y. Mukoyama, N. Mizuno, J.R. Hogg, and K. Sadtler for access to their laboratory equipment, G. Arora, R. Pavani, F.E. Clark, L.F. Rosin, V. Sundaresan, and W. Li for technical advice, A. Nussenzweig for the 53BP1 antibody, R.E. Vance for the SP140 antibody, NHLBI Transgenic Core (C. Liu) for embryo transfer experiments, and NIH building 14F animal facility staff for the care with our mouse colony,

especially the “jumpy” mice. The contributions of the NIH authors are considered Works of the United States Government. The findings and conclusions presented in this paper are those of the authors and do not necessarily reflect the views of the NIH or the U.S. Department of Health and Human Services.

Funding: Division of Intramural Research at the National Institutes of Health/National Heart, Lung, and Blood Institute (1ZIAHL006249) to TA.

Author contributions: Conceptualization: DMZAS and TA; Methodology: DMZAS, MS, TT; Investigation: DMZAS, MS, TT, TA; Funding acquisition: TA; Supervision: TA; Writing – original draft: DMZAS; Writing – review & editing: DMZAS, MS, TT, TA.

Declaration of interests: Authors declare that they have no competing interests.

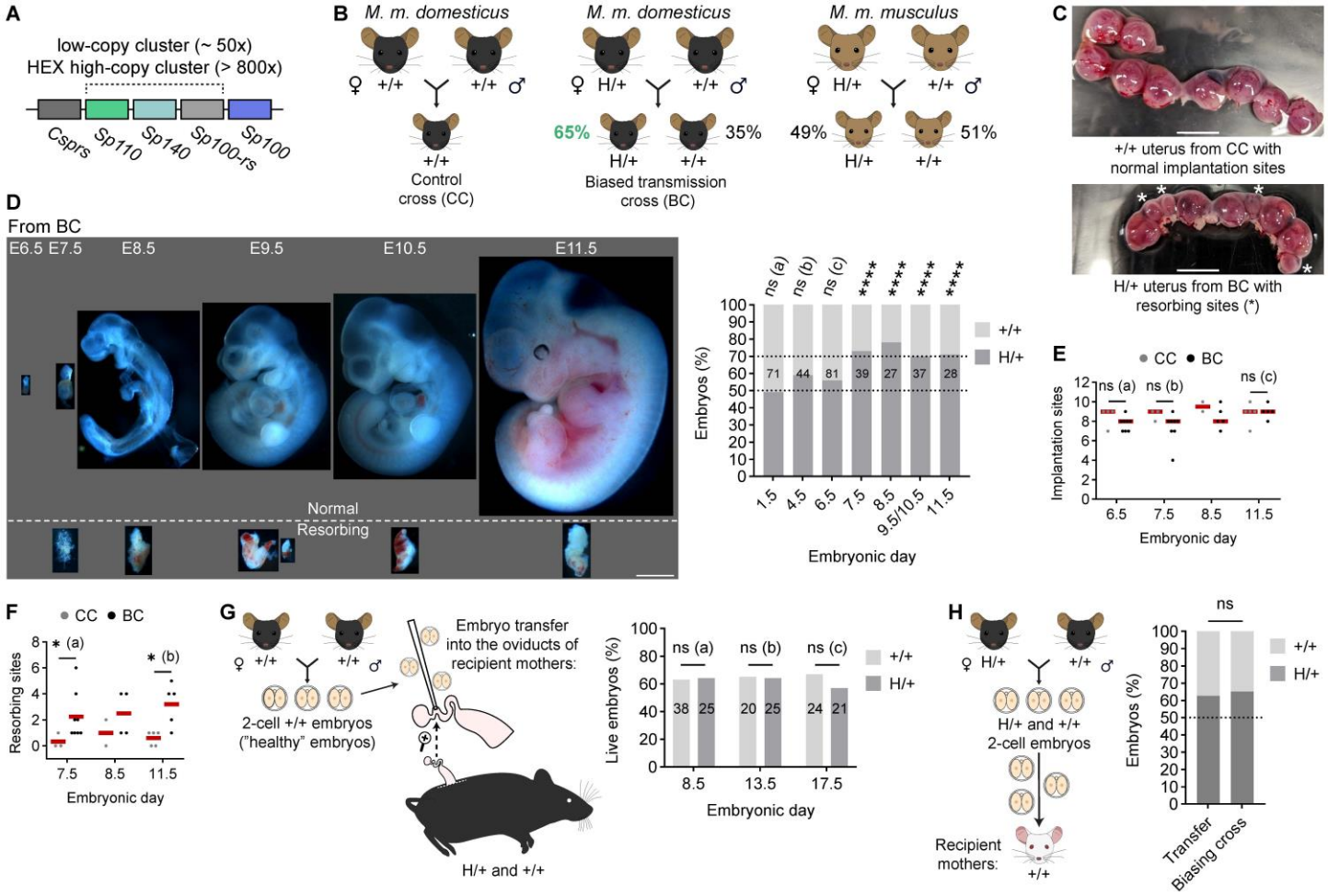

Figure 1 Selfish HEX kills wild-type embryos by causing internal issues. (A) Simplified diagram of the HEX locus (high-copy repeat) and wild-type low-copy repeat based on Weichenhan, D. et al.[56] **(B)** Schematic of different crosses to study HEX transmission. **(C)** Uterus from the control cross (CC) with regular implantation sites and from the biasing cross (BC) with resorbing sites (*); scale bars, 500 μm. **(D)** Time-course embryo dissection showing normal and resorbing embryos from the biasing cross; E, embryonic day; scale bar, 1 mm. Graph is a quantification of genotype ratios (H/+ versus +/+) at each time point; total number of embryos analyzed are indicated on top of each bar; Binomial test (two-sided) was used to examine deviation from the Mendelian expectation (50:50); ns (a) = 0.9204, ns (b) =0.0886, ns (c) = 0.2713, ****$P < 0.0001$. **(E)** Numbers of implantation sites in the control cross (CC) and the biasing cross (BC) were quantified; n = 4, 8, 3, 8, 2, 5, 5, and 5 females from left to right groups; Mann-Whitney test (two-sided) was used for statistical analysis; ns (a) = 0.2788, ns (b) = 0.1636, ns (c) = 0.9524. **(F)** Numbers of resorbing sites in CC and BC were quantified; n = 3, 8, 2, 4, 5, and 5 females for E6.5 CC, E6.5 BC, E7.5 CC, E7.5 BC, E8.5 CC, E8.5 BC, E11.5 CC, and E11.5 BC, respectively; Mann-Whitney test (two-sided) was used for statistical analysis; *(a) $P = 0.0485$, *(b) $P = 0.0317$. **(G)** Schematic of the first embryo transfer experiment using healthy two-cell embryos from CC (left); percentages of live embryos relative to total

implantation sites were quantified for each recipient mother's genotype, +/+ and H/+, at different timepoints; number of embryos analyzed is indicated on top of each bar; Chi-square test (two-sided) was used for statistical analysis; ns (a) = 0.9458, ns (b) = 0.9445, ns (c) = 0.5109. **(H)** Schematic of the second embryo transfer experiment using two-cell embryos from BC (left); The genotype ratio of transferred embryos was compared to natural biasing cross (the data for natural cross is from Table 1); n = 51, 287 for Transfer and Biasing cross, respectively; Binomial test (two-sided) was used for statistical analysis; ns = 0.7692.

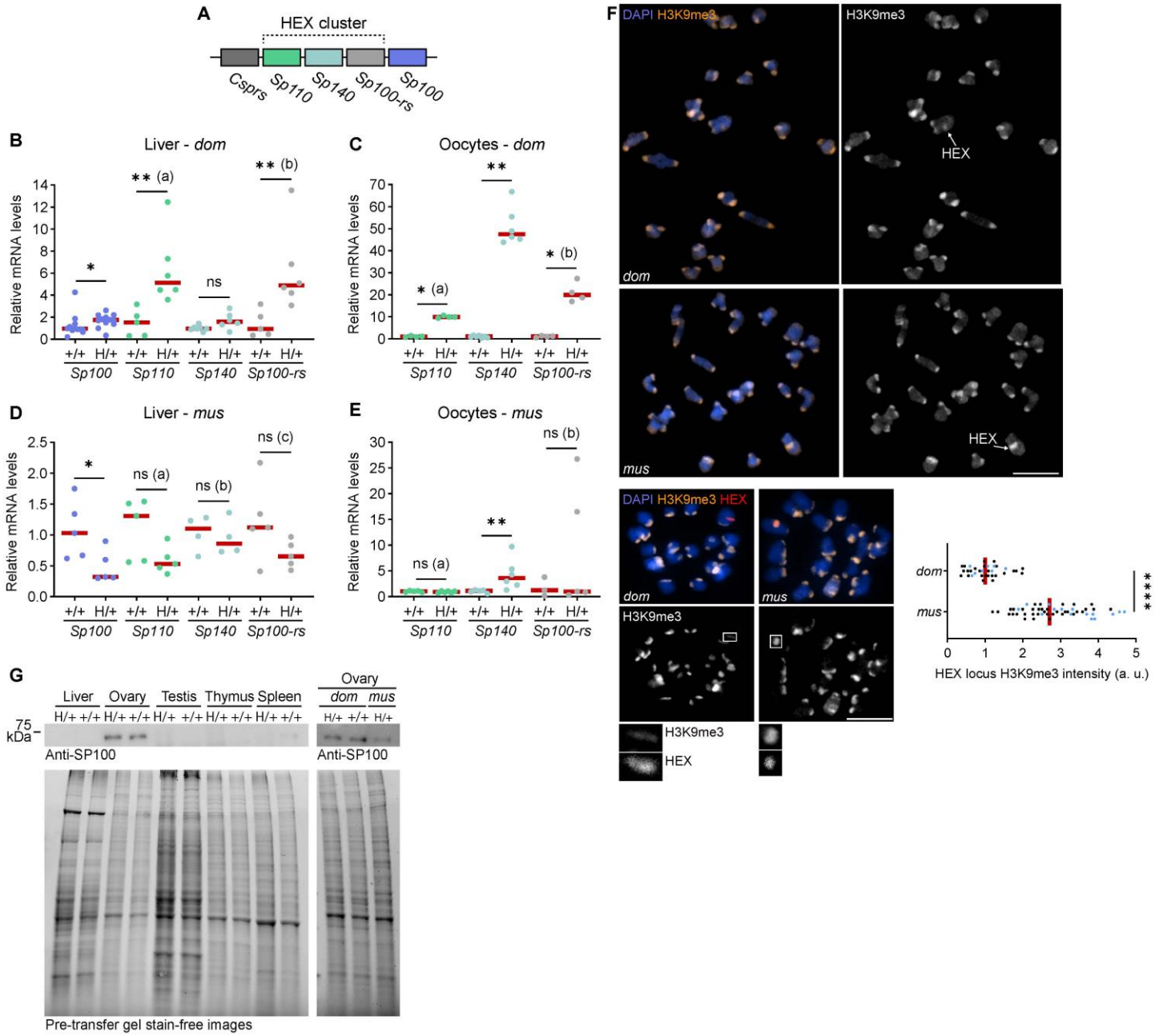

Figure 2 No HEX gene expression, no biased transmission. (A) Simplified diagram of HEX repeats based on Weichenhan, D. et al.[56] **(B)** Transcript levels of HEX genes in +/+ and H/+ *Mus musculus domesticus* (*dom*) liver were analyzed by RT-qPCR; Mann-Whitney test (two-sided) was used for statistical analysis; n = 12, 12, 5, 6, 7, 6, 5, and 6 for samples from left to right groups. Data for *Sp100* was pooled from two independent experiments. *P = 0.0242, **(a) P = 0.0043, ns = 0.0513, **(b) P = 0.0087; red line, median. **(C)** Transcript levels of HEX genes in +/+ and H/+ *dom* oocytes analyzed by RT-qPCR; Mann-Whitney test (two-sided) was used for statistical analysis; n = 4, 4, 7, 6, 4, and 4 for samples from left to right groups. *(a) P = 0.0286, **P = 0.0012, *(b) P = 0.0286; red line, median. **(D)** Transcript levels of HEX genes in +/+ and H/+ *Mus musculus musculus* (*mus*) liver analyzed by RT-qPCR; Mann-Whitney test (two-sided)

was used for statistical analysis; n = 5, 5, 5, 5, 4, 4, 5, and 5 for samples from left to right groups. *P = 0.0317, ns (a) P = 0.0952, ns (b) P = 0.8857, ns (c) P = 0.1508; red line, median. **(E)** Transcript levels of HEX genes in +/+ and H/+ *mus* oocytes analyzed by RT-qPCR; Mann-Whitney test (two-sided) was used for statistical analysis; n = 5, 6, 5, 6, 3, and 5 for samples from left to right groups. ns (a) = 0.329, **P = 0.0087, ns (b) = 0.7857; red line, median. In BE**,** comparisons are made within each gene, and the values are not intended for comparisons across different genes. **(F)** H/+ oocytes from *dom* and *mus* were fixed at prometaphase I and stained for H3K9me3 (top). H3K9me3 signal intensities at the HEX locus were quantified; datapoints from two independent experiments are indicated by dots with distinct colors; n = 34 and 51 for *dom* and *mus*, respectively; Welch's t test (two-sided) was used for statistical analysis; ****P < 0.0001; red line, median. Images are sum intensity Z-projections showing all chromosomes; scale bar, 10 μm. H/+ oocytes from *dom* and *mus* were fixed at prometaphase I and stained for H3K9me3, followed by FISH using the HEX probe (bottom). Images are sum intensity Z-projections showing all chromosomes; scale bar, 10 μm, scale bar of enlarged insets, 1 μm. **(G)** Western blot of SP100 using tissue samples from H/+ and +/+ *dom* (left) and *dom* and *mus* (right). As a loading control, stain-free gel images are shown; see Figure S2 for gel source data.

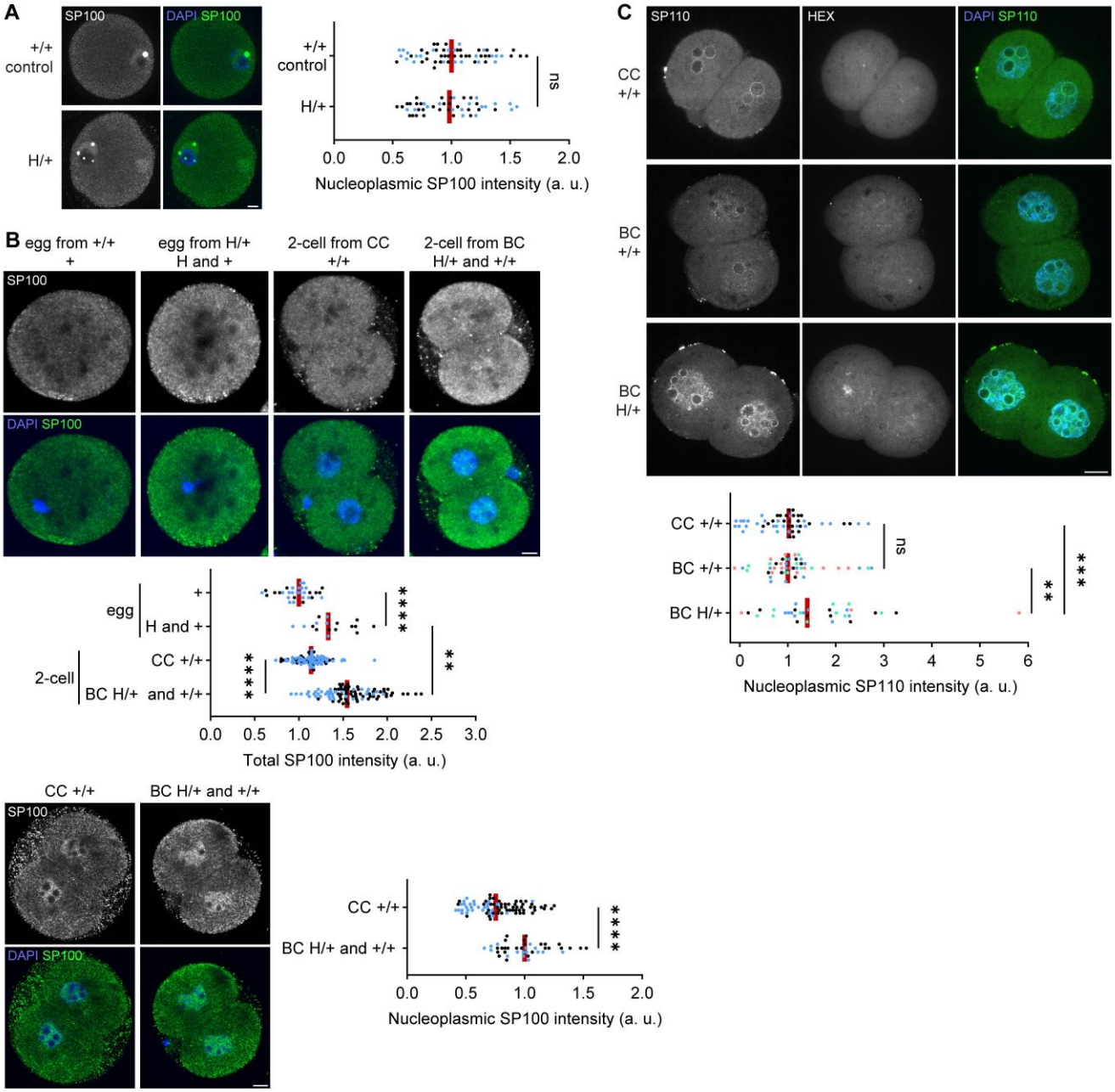

Figure 3 Toxin is deposited in all embryos while the antidote is private to HEX embryos. **(A)** Oocytes were fixed at the germinal vesicle (GV) stage and stained for SP100. The signal intensities were quantified; n = 58 and 47 for +/+ control and H/+, respectively; Mann-Whitney test (two-sided) was used for statistical analysis; ns = 0.3912; red line, median; dots, individual cells from two-cell embryos. Images are maximum intensity Z-projections; scale bar, 10 μm. **(B)** metaphase II eggs and two-cell embryos were fixed and stained for SP100. The total signal intensities in each cell were quantified (top) (n = 31, 17, 100, and 92 for + egg, H and + egg, CC +/+ 2-cell, BC H/+ and +/+ 2-cell, respectively). Welch's t test (two-sided) was used for statistical analysis; ****$P < 0.0001$, **$P = 0.0063$; red line, median; dots, individual cells. Nucleoplasmic signal intensities were quantified in two-cell embryos (bottom) (n = 80 and 42 for

604 CC +/+ and BC H/+ and +/+, respectively); Mann-Whitney test (two-sided) was used for
605 statistical analysis; ****$P < 0.0001$; red line, median; dots, individual cells. Images are
606 maximum intensity Z-projections; scale bar, 10 μm. **(C)** Embryos were fixed at the late two-cell
607 stage, stained for SP110, and genotyped by FISH with the HEX probe. The signal intensities
608 were quantified (n = 50, 47, and 33 for CC +/+, BC +/+, and BC H/+, respectively). Mann-
609 Whitney test (two-sided) was used for statistical analysis; ns = 0.3368, **$P = 0.0037$, ***$P =$
610 0.0004; red line, median; dots, individual cells. This experiment was independently repeated two
611 times for CC +/+ and four times for BC +/+ and BC H/+. Images are maximum intensity Z-
612 projections; scale bar, 10 μm. Data points from two or more independent experiments are
613 indicated by dots with distinct colors.
614

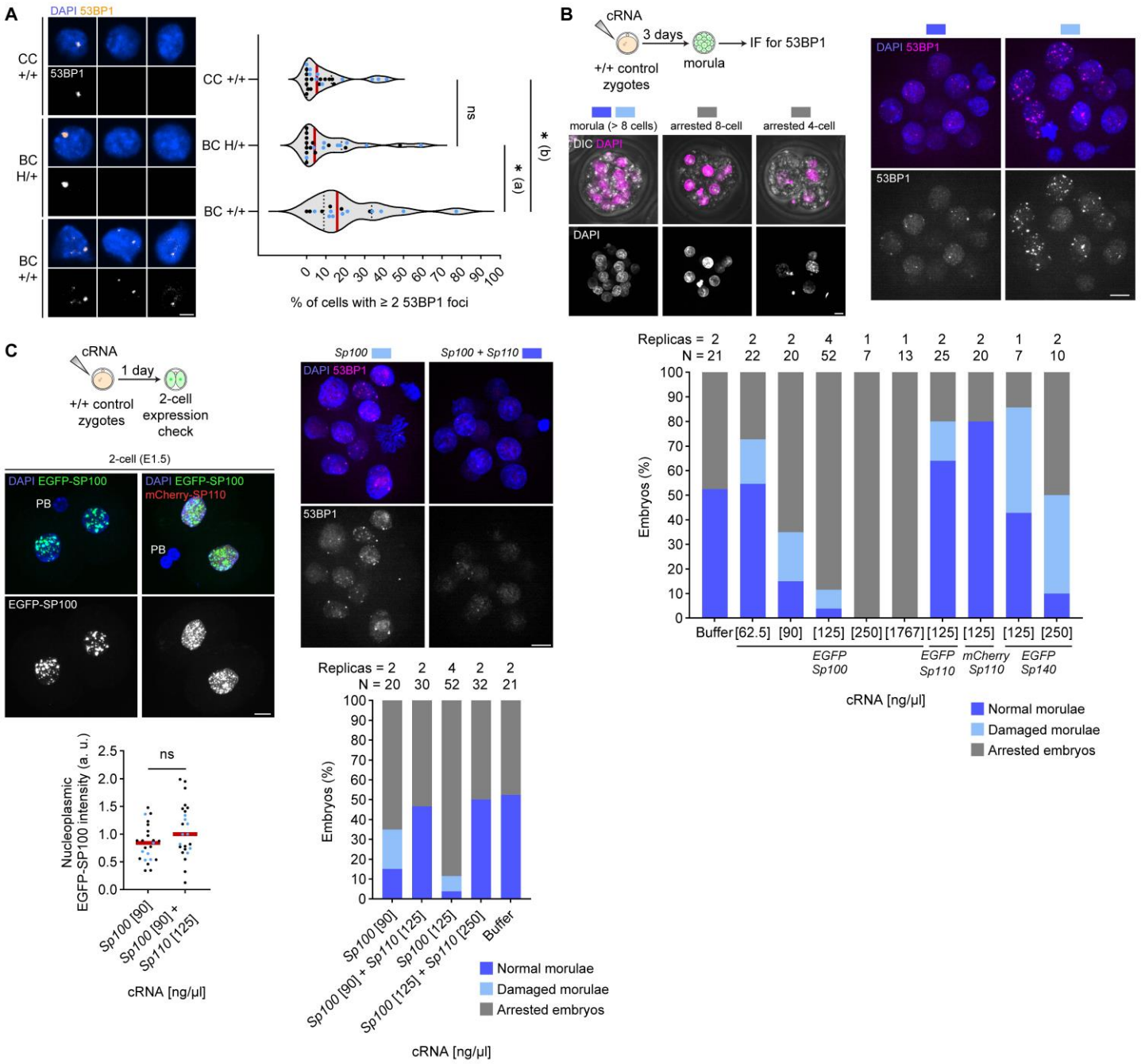

Figure 4 SP100 and SP110 consist a minimal toxin-antidote module, sabotaging mammalian embryogenesis. (A) Embryos from control cross (CC) and biasing cross (BC) were fixed at E6.5 and stained for 53BP1. Percentages of cells with more than two 53BP1 foci in each embryo were quantified; Mann-Whitney test (two-sided) was used for statistical analysis; ns = 0.9691, *(a) $P = 0.0254$, *(b) $P = 0.0102$; red line, median; dots, percentage per embryo. Data points from two independent experiments are indicated by dots with distinct colors (n = 24, 22, 16 embryos for CC +/+, BC H/+, and BC +/+, respectively). **(B)** Zygotes were microinjected with cRNA, cultured for three days (E3.5), and fixed to stain for 53BP1. Embryos at the morula

stage (> eight cells) were classified as normal morulae (< two cells within the embryo with five or more 53BP1 foci, dark blue) or damaged morulae (two or more cells with five or more 53BP1 foci, light blue), and embryos with eight cells or fewer were classified as arrested embryos (grey). Proportions of embryos in each category were quantified; sample size and the number of independent experiments are shown above each bar in the graph. **(C)** Embryos expressing EGFP-SP100 and mCherry-SP110 were fixed at the two-cell stage and counterstained with DAPI. EGFP-SP100 nucleoplasmic signal intensities were quantified as a readout of expression levels; datapoints from two independent experiments are indicated by dots with distinct colors; n = 23 and 24 for *Sp100* [90] and *Sp100* [90] + *Sp110* [125], respectively; Welch's t test (two-sided) was used for statistical analysis; ns = 0.0625; red line, median; dots, individual cells. Similarly, embryos expressing EGFP-SP100 and mCherry-SP110 were cultured for three days, fixed and stained for 53BP1, and categorized as in B (bottom); note that data for *Sp100* [90], *Sp100* [125], and Buffer are from the graph in B; sample size and the number of independent experiments are shown above each bar. Images in this figure are maximum intensity Z-projections except for the ones with DIC, which are standard deviation intensity Z-projections; PB, polar body; scale bar, 10 μm.

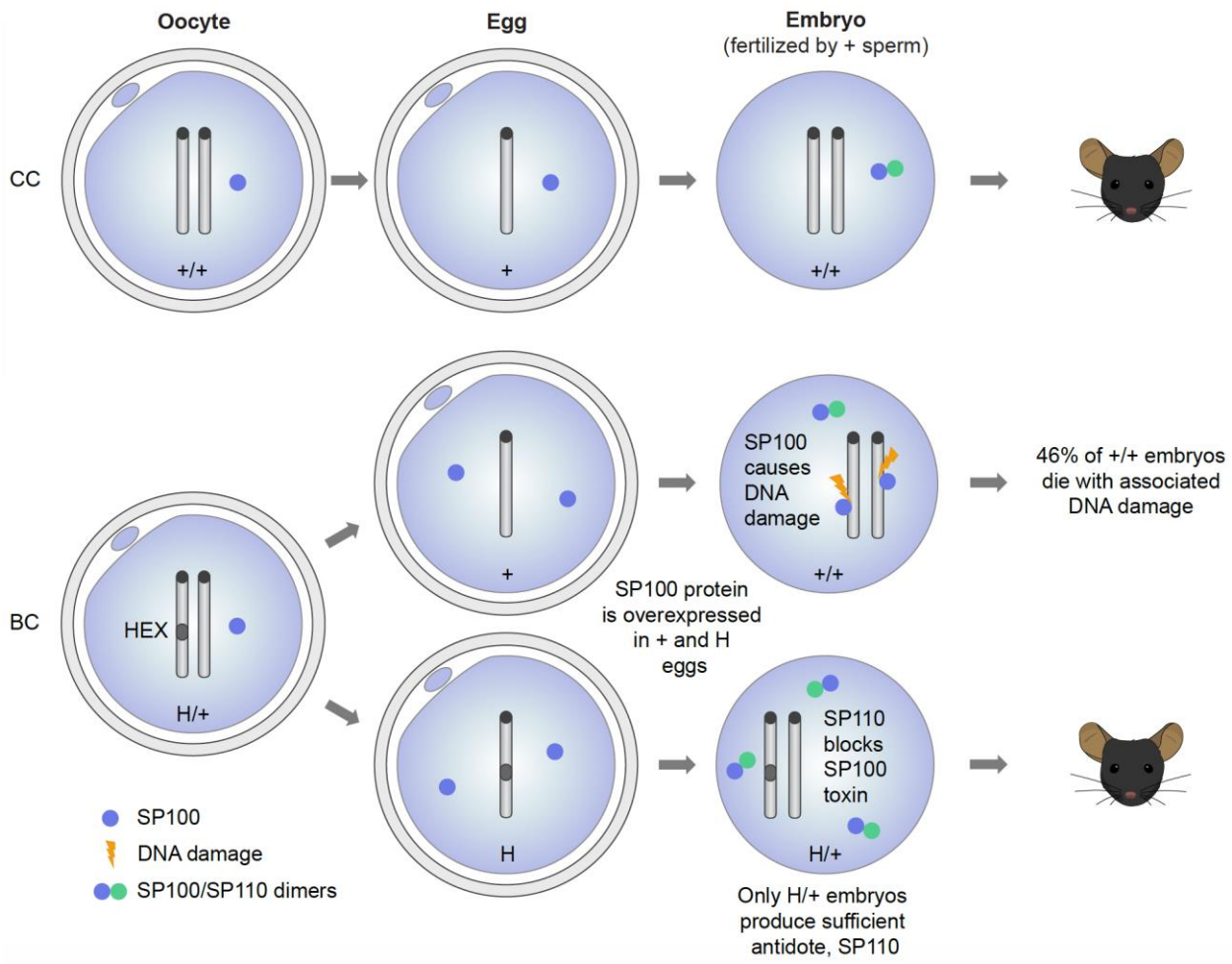

Figure 5 HEX represents the first canonical toxin-antidote system in vertebrates. SP100 toxin becomes enriched in eggs and early embryos from H/+ females. SP100 levels are elevated in all embryos from biasing crosses (BC), regardless of genotype. In contrast, SP110 antidote is selectively upregulated in H/+ embryos following fertilization. This differential expression provides a mechanism by which only HEX-positive embryos neutralize genotoxicity. Although the t-haplotype meiotic drive system in male mice has occasionally been categorized as a TA-like system, it involves multiple distorters and a responder, and therefore mechanistically, it is a distorter-responder system. In contrast, HEX employs a tightly linked two-gene toxin-antidote module, characteristic of a canonical TA system. In human cells, the SP100-SP110 interaction via the CARD domain is crucial for neutralizing the cytotoxicity of SP100 overexpression (Figure S6B).[28] Neutralization through the toxin-antidote direct interaction is another feature of canonical TA systems. Therefore, we believe HEX represents the first canonical TA system in vertebrates.

654 **Experimental model details**
655
656 Mouse strains and crossing schemes
657 Mouse strains were purchased from the Jackson Laboratory (B6.Cg-Is(HSR;1)1Lub/J,
658 stock# 001914, *Mus musculus domesticus* with the HEX locus on chromosome 1, C57BL/6J,
659 stock# 000664, *Mus musculus domesticus*, PWD/PhJ, stock# 004660, *Mus musculus musculus*)
660 or Charles River (CD-1® IGS, stock# 022, *Mus musculus domesticus*). The HEX locus was
661 introduced to the *M. m. musculus* background by backcrossing H/+ *M. m. domesticus* mice with
662 +/+ *M. m. musculus* (PWD/PhJ) mice for six generations. HEX transmission was measured by
663 crossing H/+ *dom* females and +/+ *dom* males or by crossing H/+ *mus* females from the
664 backcrosses and +/+ *mus* males. Mice were maintained in an animal facility under a 12-hour
665 light/dark cycle at room temperature, with minimal disturbance and humidity ranging from 30%
666 to 70% depending on the season. All animal experiments were conducted in accordance with the
667 National Institutes of Health guidelines and approved by the Animal Care and Use Committee
668 (Animal Study Proposal Numbers: H-0327 and H-0125).
669
670 **Method details**
671
672 Mouse oocyte and egg collection and culture
673 For oocyte collection, 6-12 week old *M. m. domesticus* females were primed with 7.5 U
674 of pregnant mare serum gonadotropin (PMSG, Medix Biochemica, cat# 493-10) 44-48 hour
675 before collection, while *M. m. musculus* females were primed with 5 U of CARD HyperOva
676 (Cosmo Bio, cat# KYD-010-06-EX) 44-48 hour before collection. For metaphase II egg
677 collection, the females were also primed with 7.5 IU of hCG (Millipore, Cat# 9002–61-3 C1063)
678 48 hours after the PMSG injection and euthanized 17 hours after the hCG injection. Germinal
679 vesicle (GV) oocytes were collected in M2 media (Sigma, cat# M7167) with 2.5 mM milrinone
680 (Sigma, cat# 475840) to inhibit meiotic resumption. Oocytes were then transferred to M16 media
681 (Millipore, cat# M7292) with 2.5 mM milrinone covered with parafin oil (Nacalai, cat#
682 NC1506764) in a humidified atmosphere of 5% CO_2 in air at 37°C. For prometaphase I analysis
683 (Figure 2F), milrinone was washed out to allow meiotic resumption. The oocytes were then fixed
684 3 hours after milrinone washout. Eggs were collected in M2 media from the ampulla of 4-12
685 week old females, transferred to M16 media covered with paraffin oil, and incubated at 37°C in a
686 humidified atmosphere of 5% CO_2 in air. Oocyte and egg manipulations were performed in a
687 Petri dish (Falcon, cat# 351007).
688
689 *In vitro* fertilization to obtain zygotes
690 Zygotes were obtained by IVF following the Nakagata method,[57] using +/+ *dom* sperm
691 and H/+ or +/+ *dom* eggs, except that eggs were collected in HTF media (Millipore, cat# MR-
692 070-D). Cumulus cells and sperm were washed out 4-6 hours after fertilization in HTF media,
693 and zygotes were transferred to KSOM media (Millipore, cat# MR-106) under paraffin oil.
694 Zygote pronuclei were examined with an M80 stereo microscope (Leica, cat# 01-672-670) with a
695 Thermo Plate TPX (Leica). Embryos with anormal pronuclei numbers and unfertilized eggs were
696 discarded. Zygotes were cultured at 37°C in a humidified atmosphere of 5% CO_2 in air to reach
697 various stages.
698
699 Post-implantation embryo collection

700 Embryos were dissected from H/+ *dom* pregnant females naturally mated with +/+ *dom*
701 males. Dissections were performed during embryonic days E6.5 to E11.5 following standard
702 laboratory protocols.[57,58] Embryos were placed in HBSS media (Gibco, cat# 14175095) and
703 imaged using the MZ16F stereomicroscope (Leica) and the Leica Application Suite X software.
704 After imaging, embryos were frozen at -70°C until genotyping (see below).
705
706 DNA isolation and genotyping by qPCR
707 Genomic DNA (gDNA) was extracted from tail snips following the HotSHOT protocol.[59]
708 Samples were genotyped by measuring the relative quantification (RQ) of the *Sp100-rs* gene by
709 qPCR. RQ was estimated through the $2^{-\Delta C_T}$ method[60] using the *36b4* gene as a reference (Table
710 S1). Primers were designed using a modified version of Primer3 2.3.7[61] implemented in
711 Geneious 10.2.6 (Biomatters) (Table S1). The presence of the *Sp140* gene in the HEX locus
712 (Figure S1) was also tested with a specific primer set (Table S1) using the *36b4* gene as a
713 reference. Quantitative PCR was performed on a LightCycler 96 (Roche). Reactions were
714 performed at a final volume of 10 µl, with 60 ng of gDNA, 5 µl of iTaq Universal SYBR Green
715 Supmix (Bio-Rad, cat# 1725121), and 1 µl of each 5 µM primer. Cycle conditions were 95°C for
716 10 min; 40 cycles of 95°C for 5 s and 60°C for 20 s. Target and reference genes were analyzed
717 simultaneously in triplicate. The specificity of the PCR products was confirmed by dissociation
718 curve analysis. We estimated the amplification efficiency (E) of each primer set by standard
719 curve performed on a 5-fold dilution series of gDNA. Amplification efficiencies were E*Sp100-rs*
720 = 100% and E*36b4* = 96%, which are acceptable to use for the $2^{-\Delta C_T}$ method without correction.
721 We classified animals as wild-type, heterozygous for HEX, and homozygous for HEX,
722 comparing their RQ values with those obtained from animals with known genotypes. Animals
723 with inconsistent RQ values were excluded from any following experiments. E1.5 to E7.5
724 embryos were genotyped by FISH using an HEX probe (see below).
725
726 Oligopaint design and genotyping by FISH
727 We manually designed a set of probes for the HEX locus. Probes were designed at the
728 *Sp100-rs* and *Sp110* exons and were synthesized by Integrated DNA Technologies. E1.5-E4.5
729 embryos produced by natural crosses were spread onto microscope slides based on the standard
730 protocol.[62,63] Briefly, embryos were treated with a hypotonic solution (0.1% sodium citrate in 0.2
731 mg/ml BSA), transferred to a hypotonic solution drop onto the microscope slide, and air dried.
732 Just before completely dried, 8 µl of spreading solution (0.1% Tween-20 in 0.01 N HCl) was
733 added over the cells and allowed to dry for about 1 hour. Cells were then fixed using a 1:3
734 mixture of acetic acid/methanol and let air dry. The FISH process was performed following the
735 procedures described in Clark et al[64] using 100 pmol of the HEX primary probe. E6.5 and E7.5
736 embryos were spread and genotyped by FISH as described in "Immunostaining and FISH on
737 E6.5 embryos" (see below).
738
739 Western blot
740 Liver, ovary, testis, thymus, and spleen samples were dissected, flash frozen in liquid
741 nitrogen, and stored at -70°C. To extract protein from dissected tissues, 50 mg of each sample
742 were homogenized using RIPA buffer (150 mM NaCl (Millipore, cat# 116224), 0.5% Sodium
743 deoxycholate (Biochemica, cat# A1531), and 50 mM Tris, pH 8.0 (KD Medical, cat# RGF-
744 3360), and 1% Triton X-100) supplemented with the protease inhibitor cocktail (MedChem
745 Express, cat# HY-K0010). Extracts were mixed with Laemmli buffer (BioRad, cat# 1610737)
746 containing 2-mercaptoethanol (VWR Life Sciences, cat# 97064-590) and denatured at 95°C for 5
747 min. Samples were separated on 10% Mini-Protean TGX Stain-Free Protein Gels (Bio-Rad, cat#

4568035) to visualize the total proteins with the ChemiDoc MP Imaging System (Bio-Rad, cat# 12003154). Proteins were then transferred to the PVDF membrane (Bio-Rad, cat# 1704156) with the Trans-Blot Turbo System (Bio-Rad, cat# 1704150). The membrane was blocked for 1 hour at RT with 2% Membrane Blocking agent (Cytiva, cat# RPN2125), incubated overnight at 4°C with the mouse anti-human SP100 (1:1000, Santa Cruz, cat# sc-293458), and washed three times for 15 min each with the TBST buffer (20 mM Tris, pH 7.6, 150 mM NaCl, and 0.1% Tween-20). The membrane was then incubated for 1 hour with the Goat Anti-Mouse IgG-heavy and light chain cross-adsorbed Antibody HRP conjugated (1:10,000 Bethyl, cat# A90-516P), followed by three 15 min washes with the TBST buffer. SP100 protein was visualized using the ECL detection reagents (Bio-Rad, cat# 1705062) and ChemiDoc MP Imaging System.

Immunostaining of whole oocytes, eggs, and two-cell embryos

Oocytes at the germinal vesicle stage (GV) or prometaphase I (3 hour from milrinone washout), meiosis II eggs, and early two-cell embryos were fixed in freshly prepared 2% paraformaldehyde (Electron Microscopy Sciences, cat# 15710) in 1x PBS (Quality Biological, cat# 119-069-101CS) with 0.1% Triton X-100 (Millipore, cat# TX1568–1) for 20 min at room temperature (RT), washed in blocking solution (0.3% BSA (Fisher bioreagents, cat# BP1600–100) and 0.01% Tween-20 (ThermoFisher, cat# J20605-AP) in 1x PBS) for 10 min at RT, permeabilized in 1x PBS with 0.1% Triton X-100 for 15 min at RT, incubated in the blocking solution for 15 min at RT, incubated for 1 hour with primary antibodies at RT, washed three times for 10 min with the blocking solution, incubated for 1 hour with secondary antibodies at RT, and washed three times for 10 min in the blocking solution. GV oocytes, eggs, and two-cell embryos were incubated for 30 min with Antifade Mounting Medium with DAPI (Vector Laboratories, cat# H-1200) diluted 1:1 in the blocking solution and placed into 3 µl drops of the blocking solution covered with paraffin oil in a glass-bottom tissue culture dish (fluoroDish, cat# FD35–100). Oocytes at prometaphase I were mounted on microscope slides with Antifade Mounting Medium with DAPI. The following primary antibodies were used: rabbit anti-mouse SP100 antibody (Figures 3A, 3B, and S3, 1:100, custom serum raised by LabCorp), rabbit anti-human SP140 antibody (Figure S6A, 1:100, Invitrogen, cat# PA5-110417), and rabbit anti-Histone H3K9me3 antibody (Figure 2F, 1:100, Abcam, cat# ab8898). Secondary antibodies used were Alexa Fluor 488–conjugated donkey anti-rabbit (1:500, Invitrogen, cat# A21206), and Alexa Fluor 568–conjugated donkey anti-rabbit (1:500, Invitrogen, cat# A10042).

Immunostaining and Oligopaint FISH of mouse oocytes and embryos

Immunostaining combined with FISH for mouse oocytes and two-cell embryos followed our recently developed protocol.[64] Briefly, prometaphase I oocytes and two-cell embryos were immunostained with rabbit anti-Histone H3K9me3 antibody (Figure 2F, 1:100, Abcam, cat# ab8898) and Alexa Fluor 568–conjugated donkey anti-rabbit (1:500, Invitrogen, cat# A10042) secondary antibody. Two-cell embryos were immunostained with mouse anti-mouse SP110 (Figure 3C, 1:33, Santa Cruz, cat# sc-376345) or rabbit anti-mouse SP100 antibody (Figure S3, 1:100, custom serum raised by LabCorp) as a primary antibody and Alexa Fluor 488–conjugated donkey anti-rabbit (1:500, Invitrogen, cat# A21206) or Alexa Fluor 488–conjugated donkey anti-mouse (1:500, Invitrogen, cat# A21202) as a secondary antibody. Embryos were incubated overnight at 4°C in the primary antibody for the SP110 staining or 1 hour at RT for the SP100 staining. The blocking solution used for this immunostaining was (0.3% BSA and 0.01% Tween-20 in 1x PBS). Subsequent FISH used 100 pmol of the HEX probe. To improve the retention rate of embryos on the microscope slide, we made the following modification to the original protocol.[64] Prior to attaching embryos to the slide, embryos were washed in 1x PBS in ultra-low

796 attachment microplates (Corning Costar, cat# 07-200-601) to prevent adhesion to the dish.
797 Embryos were then transferred to a 1x PBS drop on Fisherbrand ColorFrost Plus microscope
798 slides (Fisher Scientific, cat# 12-550-16A), instead of poly-L-lysine treated slides,[64] allowing
799 them to attach. After PFA fixation,[64] slides were washed three times for 5 min with 10 ml of 1x
800 PBS while placing the slides horizontally on the bench (instead of inserting them vertically into
801 cuplin jar), which minimizes embryo detachment from the slide. The remaining FISH procedure
802 followed the original protocol.[64]
803
804 Immunostaining and FISH on E6.5 embryos
805 Following natural mating, embryos were dissected at E6.5 as described above. After
806 dissection, the ectoplacental cones were removed using 27G needles, and embryos were washed
807 in three drops of 1x PBS to avoid contamination of maternal tissues. Embryonic cells were then
808 spread on microscopy slides in the fixative solution (4% PFA and 0.01% Tween-20 in 1x PBS).
809 Cells were mechanically dissociated by pipetting up and down using a mouth-operated pipette.
810 The PFA solution was allowed to dry, and the slides were frozen at -20°C. Each embryo was
811 spread within a ring made with rubber cement (Elmer's, cat# E904) on the slide using a 1 ml
812 syringe with a 27G needle.
813 For immunostaining, slides were thawed and briefly washed three times in 1x PBS and
814 incubated in the blocking solution (10% BSA, 0.01% Tween-20 in 1x PBS) for 1 hour at RT in a
815 humidified chamber. The slides were then incubated with a rabbit anti-human 53BP1 antibody
816 (Figure 4A, 1:2000, Invitrogen, cat# PA1-16565) for 1 hour at RT, washed three times with 1x
817 PBS for 10 min, incubated with Alexa Fluor 647–conjugated donkey anti-rabbit (1:500,
818 Invitrogen, cat# A32795) in the blocking solution (2% BSA, 0.01% Tween-20 in 1x PBS), and
819 washed three times with 1x PBS for 10 min. Rubber cement rings were removed using a fine
820 tweezer, and slides were mounted with Antifade Mounting Medium with DAPI. After imaging
821 the immunostained slides, coverslips were removed by immersion in 1x PBS to proceed to the
822 Oligopaint FISH process. Slides were washed for 10 min in 1x PBS, dehydrated in ethanol series
823 (85%, 90%, 100%), air-dried, and aged at RT for one day. Slides were fixed with 1%
824 paraformaldehyde in 1x PBS for 10 min at RT, washed for 5 min with 1x PBS at RT, dehydrated
825 in ethanol series, air dried, and the primary Oligopaint mix[64] with 100 pmol of the HEX probe
826 was mounted to the slides and sealed with rubber cement. Subsequent steps were performed as
827 described in Clark et al.[64]
828
829 Plasmid construction and cRNA synthesis
830 Plasmids were synthesized by Twist Bioscience using the plasmid In Vitro Transcription
831 (pIVT) vector[65] with N-terminal EGFP for SP100-rs, SP100, SP110, and SP140 constructs and
832 pIVT with N-terminal mCherry for the SP110 construct. Plasmid DNA linearized by NdeI (New
833 England Biolabs, cat# R0111S) were used as a template to synthesize cRNAs with the T7
834 mMessage mMachine Kit (Ambion, cat# AM1340), followed by purification using the
835 MEGAclear Kit (ThermoFisher, cat# AM1908). cRNAs were diluted in nuclease-free water to
836 adjust their concentrations for microinjection (see below).
837
838 Zygote microinjection and immunostaining
839 Zygotes were microinjected with cRNA in M2 media using a piezo-driven
840 micromanipulator, piezoXpert (Eppendorf). During microinjection, zygotes with abnormal
841 pronuclei numbers and unfertilized eggs were discarded. Following the microinjection, zygotes
842 were cultured to different stages at 37°C in a humidified atmosphere of 5% CO_2 in air. cRNAs
843 used in this study were *Egfp-Sp100-rs* (*M. m. domesticus* SP100-rs with EGFP at the N-

844 terminus) at 1743 ng/µl, *Egfp-Sp100* (*M. m. domesticus* SP100 (isoform 1) with EGFP at the N -
845 terminus) at 62.5, 90, 125, 250, and 1767 ng/µl, *Egfp-Sp110* (*M. m. domesticus* SP110 with
846 EGFP at the N-terminus) at 125 ng/µl, *mCherry*-Sp110 (*M. m. domesticus* SP110 with mCherry
847 at the N-terminus) at 125 and 250 ng/µl, and *Egfp-Sp140* (*M. m. domesticus* SP140 with EGFP at
848 the N-terminus) at 125 and 250 ng/µl. cRNAs used in co-injections were *Egfp-Sp100* at 90 ng/µl
849 and *mCherry-Sp110* at 125 ng/µl or *Egfp-Sp100* at 125 ng/µl and *mCherry-Sp110* at 250 ng/µl.
850 After culturing, embryos were imaged at E1.5 or E4.5 to examine protein expression levels.
851 Subsequently, embryos were fixed in freshly prepared 2% paraformaldehyde in 1x PBS with
852 0.1% Triton X-100 for 20 min at RT, washed in blocking solution (0.3% BSA and 0.01%
853 Tween-20 in 1x PBS) for 10 min at RT, permeabilized in 1x PBS with 0.1% Triton X-100 for 15
854 min at RT, incubated in the blocking solution (5% BSA and 0.01% Tween-20 in 1x PBS) for 1
855 hour at RT, incubated 1 hour with rabbit anti-human 53BP1 antibody (Figures 4B and 4C,
856 1:2000, Invitrogen, cat# PA1-16565) at RT, washed three times for 10 min with the blocking
857 solution (5% BSA and 0.01% Tween-20 in 1x PBS), incubated 1 hour with Alexa Fluor 647–
858 conjugated donkey anti-rabbit (1:500, Invitrogen, cat# A32795) antibody at RT, washed three
859 times for 10 min in the blocking solution (0.3% BSA and 0.01% Tween-20 in 1x PBS),
860 incubated 30 min with Antifade Mounting Medium with DAPI (Vector Laboratories, cat# H-
861 1200) diluted 1:1 in the blocking solution, and placed into 3 µl drops of the blocking solution
862 covered with paraffin oil in a glass-bottom tissue culture dish (fluoroDish, cat# FD35–100) to
863 proceed to confocal microscopy (see below).
864
865 Microscopy and image analysis
866 Fixed oocytes and embryonic cells were imaged with a microscope (Eclipse Ti; Nikon)
867 equipped with 20x / 0.75 NA objective and 100x / 1.40 NA oil-immersion objective lens, CSU-
868 W1 spinning disk confocal scanner (Yokogawa), ORCA Fusion Digital CMOS camera
869 (Hamamatsu Photonics), and 405, 488, 561 and 640 nm laser lines controlled by the NIS-
870 Elements imaging software (Nikon). Confocal images were acquired as Z-stacks at 1 or 3 µm
871 intervals. Fixed oocytes and embryos were imaged with a microscope (Eclipse Ti2-E; Nikon)
872 equipped with the 20x / 0.75 NA objective and 60x / 1.40 NA oil-immersion objective, CSU-W1
873 spinning disk confocal scanner (Yokogawa), ORCA Fusion Digital CMOS camera (Hamamatsu
874 Photonics), and 405, 488, 561 and 640 nm laser lines controlled by the NIS-Elements imaging
875 software (Nikon). Confocal images were collected as Z-stacks at 0.5, 1, or 3 µm intervals.
876 Fiji/ImageJ (NIH) was used to analyze all the images. In general, optical slices containing nuclei
877 or cells were added to produce a sum intensity Z-projection for pixel intensity quantifications.
878 For quantifications of foci, optical slices were added to produce a sum (Figure 4A) or maximum
879 intensity Z-projection (Figures 4B and 4C).
880 To quantify H3K9me3 signal intensities at the HEX locus (Figure 2F), regions of interest
881 (ROIs) were drawn to encompass the H3K9me3 signal on the chromosome 1 arm. In general,
882 H3K9me3 signals are enriched at the centromeric region of each chromosome, and the only
883 H3K9me3 focus outside the centromere corresponds to the HEX locus. The signal intensity was
884 integrated over each ROI after subtracting background signals, obtained from the average of
885 three chromosome regions near the HEX locus.
886 To quantify SP100 nucleoplasmic signal intensities in meiosis I GV oocytes and two-cell
887 embryos (Figure 3A), ROIs were drawn encompassing the SP100 nuclear signal based on the
888 DAPI staining. The signal intensity was integrated over each ROI after subtracting background
889 signals, obtained from the background outside the cell. To quantify SP100 and SP140 total signal
890 intensities in meiosis II eggs and two-cell embryos (Figures 3B and S6A), ROIs were drawn
891 encompassing the entire cell. The signal intensity was integrated over each ROI after subtracting

892 background signals, obtained from three background areas outside the cell. To quantify
893 nucleoplasmic signal intensities in two-cell embryos (Figure 3B), masking images were created
894 using DAPI staining images to specifically measure signal intensities in the nucleus. The signal
895 intensity was integrated over each slice after subtracting background signals, obtained from three
896 background areas outside of the cell. To quantify nucleoplasmic signal intensities (SP100 and
897 SP110) in IF-FISH images (Figures 3C and S3), masking images were created using DAPI
898 staining images to specifically measure signal intensities in the nucleus. Signal intensity was
899 averaged over each slice after subtracting cytoplasmic background signals. Nucleoplasmic
900 signals of EGFP-SP100 (Figure 4C) were quantified by the same method.
901 To quantify 53BP1 foci number per cell (Figure 4A), we developed a custom ImageJ/Fiji
902 macro (Supplementary Text) based on the strategy developed by the Duke Light Microscopy
903 Core (https://microscopy.duke.edu/guides/count-nuclear-foci-ImageJ). We manually counted
904 53BP1 foci number in Figures 4B and 4C, using maximum-intensity projected images. Foci with
905 ≥ 1 μm diameter were counted. We analyzed each slice when nuclei from different cells overlap.
906
907 Embryo transfer
908 Embryo transfers were performed by the NHLBI Transgenic Core at NIH. In the first
909 embryo transfer experiment (Figure 1G), +/+ zygotes were collected from +/+ females mated
910 with +/+ males and cultured for one day to reach the two-cell stage. Two-cell embryos were then
911 transferred to pseudo-pregnant H/+ *dom* females (mated with vasectomized males prior to the
912 transfer). As a control, embryos were also transferred to pseudo-pregnant +/+ females. Embryos
913 were dissected from these females at E9.5 (two +/+ and three H/+ females). The number of live
914 embryos and resorbing sites were scored to quantify embryo survival rates in the H/+ and +/+
915 uterus. A replica of this experiment was performed, and the embryos were dissected at E13.5 and
916 E17.5 (three +/+ and three H/+ females for each timepoint).
917 In a second embryo transfer experiment (Figure 1H), a mixture of +/+ and H/+ two-cell
918 embryos obtained by crossing H/+ *dom* females with +/+ *dom* males were transferred to eight
919 +/+ pseudo-pregnant *dom* females (CD-1 background). Embryos were dissected at E13.5 and
920 genotyped by qPCR as previously described. In a replica of this experiment, two-cell embryos
921 were implanted into five pseudo-pregnant females and dissected and genotyped at E14.5.
922
923 Gene expression profiling by RT-qPCR
924 Quantification of expression levels of *Sp100*, *Sp110*, *Sp140*, and *Sp100-rs* genes were
925 performed using liver and oocytes of *M. m. domesticus* and *M. m. musculus.* Dissected tissues
926 were immediately frozen in liquid nitrogen and stored at -70°C. RNA from oocytes was
927 extracted using the TRIzol Reagent (Invitrogen, cat# 15596026) and from liver using the total
928 RNA extraction kit (Norgen, cat#17200). RNA integrities were examined on 1% agarose gels.
929 RNA purities were examined using the NanoPhotometer NP80 (Implen, cat# NC2831907).
930 cDNA for each sample was synthesized using the SuperScript™ III First-Strand Synthesis
931 System (Invitrogen, cat# 18080051) using 0.8 μg per sample of total RNA, following the
932 manufacturer's instructions. Working solutions of the obtained cDNAs were produced by
933 diluting them 1:5 in RNase-DNase free water.
934 Primers were designed using a modified version of Primer3[61] implemented in Geneious
935 10.2.6. Primer sets for *Sp100*, *Sp110*, *Sp140*, and *Sp100-rs* genes (Table S1) were designed
936 spanning an exon-exon junction of each gene. Primer specificities were confirmed using the
937 Blast algorithm for short sequences.[61,66] *Sp100-rs* gene is a chimeric gene with the first three
938 exons of *Sp100* fused with *Csprs* gene. To specifically amplify *Sp100-rs*, we designed a primer
939 set spanning the junction of the 3rd exon of *Sp100* and the exon of *Csprs*, which avoids

940 amplifying *Sp100* (Figure S5C). Quantitative PCR was performed on QuantStudio 3 (Applied
941 Biosystems, cat# A28567), except for *Sp140* in *dom* oocytes samples that were performed on
942 LightCycler 96. Reactions were assembled in a final volume of 10 µl with 1 µl of cDNA, 5 µl of
943 iTaq Universal SYBR Green Supermix (Bio-Rad, cat# 1725121), and 0.5 µl of each 10 µM
944 primer. Cycle conditions were 95°C for 10 min; 40 cycles of 95°C for 5 s and 60°C for 20 s. The
945 specificity of the PCR products was confirmed by dissociation curve analysis. Target and
946 reference genes were analyzed simultaneously in triplicates for independent samples. DNA
947 contamination was examined using controls without reverse transcriptase (NRTC) and without
948 template cDNA (NTC). A five-fold serial dilution of the cDNAs was used to calculate the primer
949 sets amplification efficiency (E). An efficiency range of 90% to 110% was used to select primer
950 sets for further analysis. Cq values were corrected using the gene's efficiencies with the formula
951 CqE = Cq*(log(1+E)/log(2)).[67] The normalized relative expression quantity (NREQ) was
952 determined by the $2^{-\Delta\Delta C_T}$ method.[68] Expression levels of target genes were normalized using the
953 geometric mean of two housekeeping reference genes with subsequent normalization to the
954 average expression of the +/+ group. To select the reference genes, we used the RefFinder[69]
955 software. From five tested genes (*Atp5b*, *Gapdh*, *Hprt1*, *Rplpo*, and *Ubc*), we selected *Atp5b* and
956 *Rplpo* for *dom* liver, *Atp5b* and *Gapdh* for *mus* liver, *Atp5b* and *Hprt1* for *dom* and *mus* oocytes.
957
958 Quantification and statistical analysis
959 Data points were pooled from more than two independent experiments in most
960 experiments, and the exact number of independent experiments for each experimental group is
961 listed in Table S2. Data was analyzed using Microsoft Excel and GraphPad Prism 10. Bar
962 graphs, scatter plots, and violin plots were created with GraphPad Prism 10. Binomial test (two-
963 sided) for deviations from the expected 50:50 (Figure 1D and Table 1) or the biasing cross ratio
964 (Figure 1H), Chi-square test (two-tailed) (Figure 1G and Table 2), Mann-Whitney test (two-
965 sided) (Figures 1E, 1F, 2B–2E, 3A, 3B nucleoplasmic, 3C, 4A, S3, and S6A), and Welch's t test
966 (two-sided) (Figures 2F, 3B total, and 4C) were used for statistical analyses. Actual *P* values are
967 shown in each figure or figure legend.
968

Supplementary Text

Custom ImageJ/Fiji macro used to quantify 53BP1 foci in Figure 4A:

```
// Perform Z projection, adjust Min and Max, and split channels
run("Z Project...", "projection=[Sum Slices]");
setMinAndMax(1351, 2629);
run("Split Channels");

// Get the list of all open image windows
winList = getList("image.titles");

// Extract the name of the original image
originalImageName = getTitle();  // Get the title of the active image window (before renaming)

// Loop through each window title
for (i = 0; i < winList.length; i++) {
    title = winList[i];

    // Rename windows based on channel
    if (startsWith(title, "C1")) {
        selectWindow(title);  // Make sure to select the window before renaming
        rename("dapi");
    }
    if (startsWith(title, "C2")) {
        selectWindow(title);
        rename("foci");
    }
}

// Now work with the renamed images
selectWindow("dapi");
setAutoThreshold("Otsu dark");
run("Threshold...");
run("Analyze Particles...", "size=100-Infinity circularity=0.60-1.00 display exclude clear
summarize add");

selectWindow("foci");
setThreshold(2250.0000, 1000000000000000000000000000000.0000);
run("Convert to Mask");
run("Find Maxima...", "prominence=100 output=[Single Points]");
roiManager("Show None");
roiManager("Show All");

// Set measurements and analyze
run("Set Measurements...", "area integrated limit redirect=None decimal=3");
run("Clear Results");
roiManager("Measure");
```

```
// Create a save path using the original image name
savePath = "H:/Embryos/" + originalImageName + "_Results.csv";

// Save results using the original image name
saveAs("Results", savePath);

// Close any window starting with "C2"
for (i = 0; i < winList.length; i++) {
    title = winList[i];
    if (startsWith(title, "C3")) {
        selectWindow(title);
        close();  // Close the selected window
    }
}
selectWindow("Summary");
run("Close");
selectWindow("Threshold");
run("Close");
```

1037
1038
1039

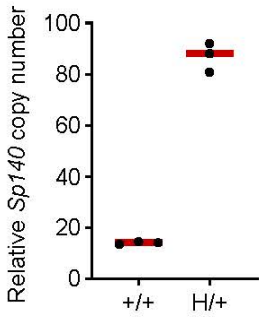

1040 **Figure S1 Relative copy number of *Sp140* in *Mus musculus domesticus* estimated by qPCR,**
1041 **related to Figure 2.** DNA samples extracted from tail snips were used to examine the copy
1042 number increase of *Sp140* gene in H/+ mice compared to +/+. See Method details "DNA
1043 isolation and genotyping by qPCR".

1044

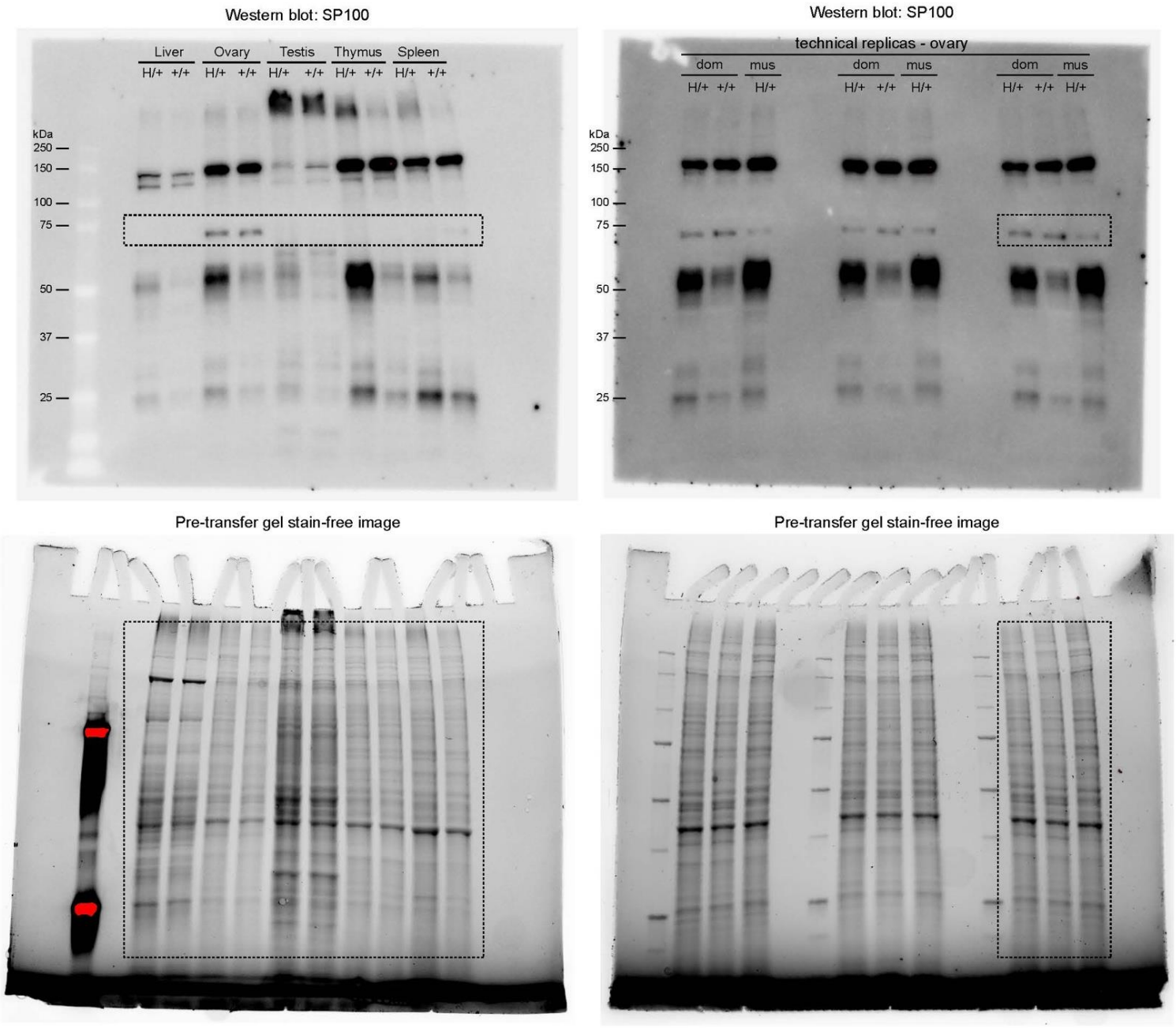

Figure S2 Uncropped images of western blots, related to Figure 2. Entire gels and membranes are imaged. Boxes in the images indicate the cropped area shown in Figure 2G.

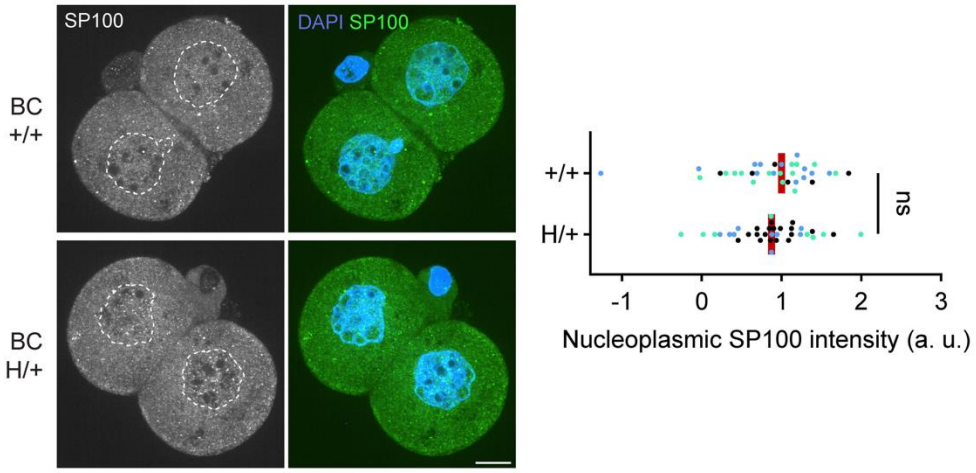

1048

1049 **Figure S3 SP100 toxin is equally deposited to +/+ and H/+ embryos, related to Figure 3.**
1050 Two-cell embryos from BC were fixed, stained for SP100 and genotyped by FISH with the HEX
1051 probe. SP100 signal intensities in the nucleus were quantified (n = 33, and 35 for +/+ and H/+,
1052 respectively). Mann-Whitney test (two-sided) was used for statistical analysis; ns = 0.5338; red
1053 line, median; dots, individual cells. This experiment was repeated independently three times,
1054 indicated by dots with distinct colors. Images are optical slices; scale bar, 10 μm.

1055

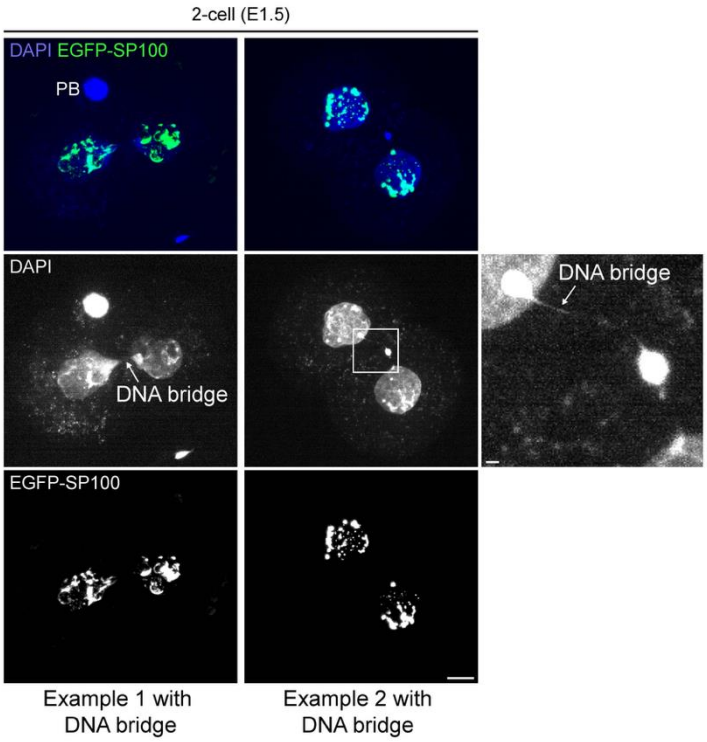

1056

1057 **Figure S4 DNA bridges induced upon SP100 overexpression in embryos, related to Figure**
1058 **4.** Embryos overexpressing EGFP-SP100 were fixed at the two-cell stage; Images are maximum
1059 intensity Z-projections; E, embryonic day; PB, polar body; scale bar, 10 μm; scale bar of
1060 enlarged inset, 1 μm.

1061

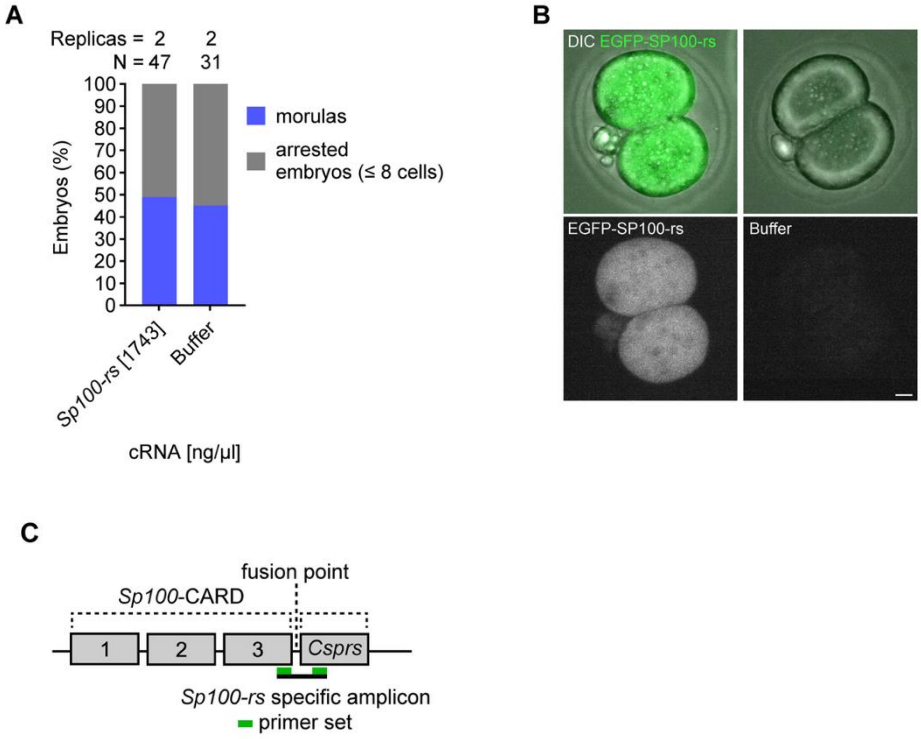

Figure S5 No significant impact on early embryogenesis upon *Sp100-rs* overexpression, related to Figure 4. (A) Control zygotes were microinjected with *Egfp-Sp100-rs* cRNA (1743 ng/µl) and cultured for three days. Embryos were categorized as normal morula (blue) or arrested embryos (grey); sample size is shown above each bar; data from two independent experiments were pooled. **(B)** Control zygotes were microinjected with *Egfp-Sp100-rs* cRNA (1743 ng/µl) or buffer and cultured for one day (the two-cell stage) to examine SP100-rs localization. Ectopically expressed EGFP-SP100-rs uniformly localized in the cell and did not show nuclear enrichment in contrast to SP100 (Figure 4C). Images are maximum intensity Z-projections; scale bar, 10 μm. **(C)** Primer designs to specifically amplify *Sp100-rs*.

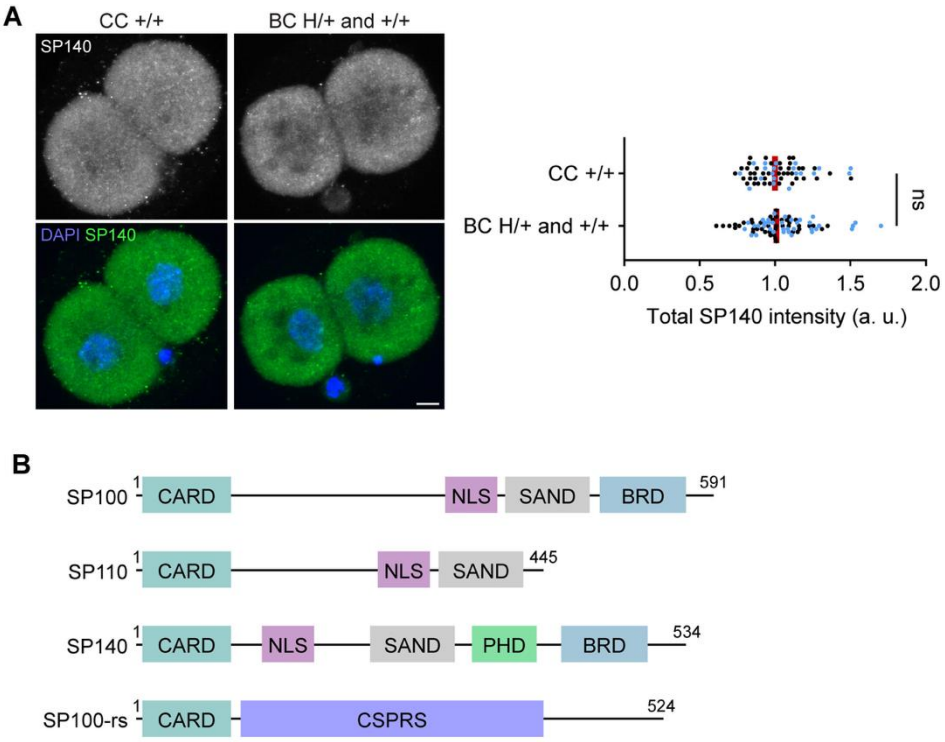

Figure S6 SP140 levels are indistinguishable in two-cell embryos from the control and biasing crosses, related to Figure 4. (A) Embryos from the control cross (CC) and the biasing cross (BC) were fixed at the early two-cell stage and stained for SP140. The signal intensities in the cell were quantified (n = 62 and 78 for +/+ CC and H/+ and +/+ BC, respectively). Mann-Whitney test (two-sided) was used for statistical analysis; ns = 0.7372; red line, median; dots, individual cells from two-cell embryos. Data points were pooled from two independent experiments, indicated by dots with distinct colors. Images are maximum intensity Z-projections; scale bar, 10 μm. **(B)** Domain organizations of the Speckled Protein (SP) family: CARD (Caspase Activation and Recruitment Domain) also known as HSR domain; NLS (Nuclear Localization Signal); SAND (named after its host proteins: SP100, Aire, NucP41/P75, and DEAF); PHD (Plant Homeodomain); BRD (Bromodomain); CSPRS (Component of *Sp100-rs*). SP100-rs does not have NLS, consistent with its uniform distribution in the cell when overexpressed (Figure S5B).

1089 **Table S1.**
1090 List of primer sets used in this study.
1091

Assay	Name	Primer (forward)	Primer (reverse)
Genotyping - qPCR	Sp100-rs	TCCACTGAACAGGAGAACACAG	ATGAATTCACGGTCTCGGAGG
	36b4[70]	ACTGGTCTAGGACCCGAGAAG	TCAATGGTGCCTCTGGAGATT
Copy number - qPCR	Sp140	ACAAGGTGGAGATCGCAAGT	GAAGTCTCGGTCTCGAAGGC
Expression - RT-qPCR	Sp100_span	ATCAGCTTGCCGAATCACCA	GTTGAGTTGCACAGCTCTTTCT
	Sp100-rs_span	GAAGCTTTGAATGTGGAGCC	CAGCCAGTCAGATACGTTGC
	Sp110_span	GACATTAAGACATCTGGAGCAGAAAG	AGGCACCCTTCTTTTGAGGT
	Sp140_span	TCGGAGCAGAAGTTTCAGGAAT	TCGTACACGACTCTCTCCACT
	Hprt1_span	CTTCCTCCTCAGACCGCTTT	CATCATCGCTAATCACGACGC
	Rplpo_span	GGACCCGAGAAGACCTCCT	GCACATCACTCAGAATTTCAATGG
	Atp5b_span	GCCACTTCCAAGGTAGCGTT	AGCAACGGTCAAACCAGTCA
	Gapdh_span	GGGTCCCAGCTTAGGTTCAT	CCCAATACGGCCAAATCCGT

1092
1093

Table S2.
List of the total numbers of events analyzed and the numbers of repeats of each experiment.

Figure 1D. Percentage of embryos genotypes per embryonic day in natural crosses

Experimental group	1.5	4.5	6.5	7.5	8.5	9.5/10.5	11.5
Number of experiments	2	3	> 13	8	4	6	5
Number of embryos	71	44	81	39	27	37	28

Figure 1E. Number of implantation sites in control and biasing crosses per embryonic days

Experimental group	6.5 CC	6.5 BC	7.5 CC	7.5 BC	8.5 CC	8.5 BC	11.5 CC	11.5 BC
Number of females	4	8	3	8	2	5	5	5

* CC +/+ x +/+, BC H/+ x +/+

Figure 1F. Number of resorbing sites in control and biasing crosses per embryonic days

Experimental group	7.5 CC	7.5 BC	8.5 CC	8.5 BC	11.5 CC	11.5 BC
Number of females	3	8	2	4	5	5

* CC +/+ x +/+, BC H/+ x +/+

Figure 1G. Percentage of live embryos after embryo transfer experiment

Experimental group	+/+ 8.5	H/+ 8.5	+/+ 13.5	H/+ 13.5	+/+ 17.5	H/+ 17.5
Number of experiments	1	1	1	1	1	1
Number of embryos	38	25	20	25	24	21

Figure 1H. Percentage of embryo genotypes after embryo transfer experiment and the biasing cross

Experimental group	Transfer	Natural cross
Number of experiments	2	42
Number of samples	51	287

1115 Figure 2B. Relative mRNA levels of HEX genes in liver - *dom*

Experimental group	+/+ *Sp100*	H/+ *Sp100*	+/+ Sp110	H/+ *Sp110*	+/+ Sp140	H/+ *Sp140*	+/+ *Sp100-rs*	H/+ *Sp100-rs*
Number of experiments	2	2	1	1	1	1	1	1
Number of samples	12	12	5	6	7	6	5	6

1116

1117 Figure 2C. Relative mRNA levels of HEX genes in oocytes - *dom*

Experimental group	+/+ *Sp110*	H/+ *Sp110*	+/+ Sp140	H/+ *Sp140*	+/+ *Sp100-rs*	H/+ *Sp100-rs*
Number of experiments	1	1	1	1	1	1
Number of samples	4	4	7	6	4	4

1118 *20-30 oocytes were pooled for each sample.

1119

1120 Figure 2D. Relative mRNA levels of HEX genes in liver - *mus*

Experimental group	+/+ *Sp100*	H/+ *Sp100*	+/+ Sp110	H/+ *Sp110*	+/+ Sp140	H/+ *Sp140*	+/+ *Sp100-rs*	H/+ *Sp100-rs*
Number of experiments	1	1	1	1	1	1	1	1
Number of samples	5	5	5	5	4	4	5	5

1121

1122 Figure 2E. Relative mRNA levels of HEX genes in oocytes - *mus*

Experimental group	+/+ *Sp110*	H/+ *Sp110*	+/+ Sp140	H/+ *Sp140*	+/+ *Sp100-rs*	H/+ *Sp100-rs*
Number of experiments	1	1	1	1	1	1
Number of samples	5	6	5	6	3	5

1123 *20-30 oocytes were pooled for each sample.

1124

1125 Figure 2F. H3K9me3 signal intensity at the HEX locus

Experimental group	*dom*	*mus*
Number of experiments	2	2
Number of cells	34	51

1126

1127 Figure 3A. SP100 nucleoplasmic signal intensity in oocytes

Experimental group	+/+ control	H/+
Number of experiments	2	2
Number of cells	58	47

1128

1129

1130 Figure 3B. SP100 total signal intensity in eggs and two-cell embryos

Experimental group	Egg from +/+ +	Egg from H/+ H and +	2-cell from CC +/+	2-cell from BC H/+ and +/+
Number of experiments	2	2	2	2
Number of cells	31	17	100	92

1131

1132 Figure 3B. SP100 nucleoplasmic signal intensity in two-cell embryos

Experimental group	CC +/+	BC H/+ and +/+
Number of experiments	2	2
Number of cells	80	42

1133

1134 Figure 3C. SP110 nucleoplasmic signal intensity in two-cell embryos

Experimental group	+/+ CC	+/+ BC	H/+ BC
Number of experiments	2	4	4
Number of cells	50	47	33

1135

1136 Figure 4A. Percentage of cells with two or more 53BP1 foci per E6.5 embryos from natural
1137 crosses

Experimental group	+/+ CC	H/+ BC	+/+ BC
Number of experiments	2	2	2
Number of embryos	24	22	16
Number of cells analyzed per embryo	28-155	22-109	19-149

1138

1139 Figure 4B. Percentage of normal and damaged morulae and arrested embryos after ectopic
1140 protein overexpression

Experimental group	Buffer	*EGFP-Sp100* [62.5]	*EGFP-Sp100* [90]	*EGFP-Sp100* [125]	*EGFP-Sp100* [250]
Number of experiments	2	2	2	4	1
Number of embryos	21	22	20	52	7
Experimental group	*EGFP-Sp100* [1767]	*EGFP-Sp110* [125]	*mCherry-Sp110* [125]	*EGFP-Sp140* [125]	*EGFP-Sp140* [250]
Number of experiments	1	2	2	1	2
Number of embryos	13	25	20	7	10

1141
1142
1143
1144
1145

1146 Figure 4C. EGFP-SP100 nucleoplasmic signal intensity in two-cell embryos

Experimental group	EGFP-Sp100 [90]	EGFP-Sp100 [90] + mCherry-Sp110 [125]
Number of experiments	2	2
Number of embryos	23	24

1147

1148 Figure 4C. Percentage of normal and damaged morulae, and arrested embryos after ectopic
1149 protein overexpression

Experimental group	EGFP-Sp100 [90]	EGFP-Sp100 [90] + mCherry-Sp110 [125]	EGFP-Sp100 [125]	EGFP-Sp100 [125] + mCherry-Sp110 [250]	Buffer
Number of experiments	2	2	4	2	2
Number of embryos	20	30	52	32	21

1150

1151 Figure S1. Relative *Sp140* copy number

Experimental group	+/+	H/+
Number of experiments	1	1
Number of samples	3	3

1152

1153 Figure S3. SP100 nucleoplasmic signal intensity in two-cell embryos

Experimental group	+/+	H/+
Number of experiments	3	3
Number of samples	33	35

1154

1155 Figure S5A. Percentage of embryos at each developmental stage after SP100-rs ectopic
1156 overexpression

Experimental group	*Sp100-rs* cRNA	Buffer
Number of experiments	2	2
Number of embryos	47	31

1157

1158 Figure S6A. SP140 total signal intensity in two-cell embryos

Experimental group	+/+ CC	H/+ and +/+ BC
Number of experiments	2	2
Number of samples	62	78

1159